Escola de Camins
Escola Tècnica Superior d'Enginyeria de Camins, Canals i Ports
UPC BARCELONATECH

Development of a large strain strategy for topology optimization

TREBALL FINAL DE

Treball realitzat per:
Inocencio Castañar

Dirigit per:
Ramón Codina
Joan Baiges

Màster en:
Numerical Methods in Engineering

Barcelona, 15/06/2018

Departament d'Enginyeria Civil i Ambiental

I would like to dedicate this thesis to my loving family and Laia.

Acknowledgements

First of all I would like to thank my advisors, Ramon and Joan, for the opportunity of joining their group and developing my master thesis with them. Since the very first moment I started here they were helping me to increase my skills. I appreciate a lot all the time they dedicated to guide me with their experience and knowledge.

I would also like to thank my work mates. Particularly Samuel for the everyday hard work during this period and the awesome rest times we took to drink a good coffee. It will be a pleasure for me to share my doctoral thesis with you, my friend.

I would finally like to specially thank my parents who made my studies possible with daily sacrifice. I could not forget my brother, my sister and Laia who are always with me when I need them.

Abstract

Topology Optimization of Nonlinear Structures has become a great challenge over the last decade. This technique looks for the optimal design of continuum and discrete structures under a set of boundary conditions and external loads. Nonlinear Solid Mechanics, studies the behaviour of structures when either the relation between strains and displacements become nonlinear or when the material behaviour must be considered nonlinear or both of them.

There are several techniques to perform Topology Optimization. Among others, the most popular ones are: the SIMP (Solid Isotropic Microstructure with Penalization) methods, which indicates the presence or absence of material through a density function, level-set methods which keep the interface tracking of the boundary and TSA (Topological Sensitivity Analysis) approaches, which study the variation of some cost function at any point of the domain.

The Topological Derivative measures the sensitivity of a given functional with respect to an infinitesimal singular perturbation, such as the insertion of holes, expansions or contraction of them and it emerges as the most powerful tool to be applied in the TSA methods.

A numerical coupling of two recent methods in shape and topology optimization of structures is proposed. The Topological Derivative concept is used in combination with a level-set method to solve the Topology Optimization problem of Nonliner Structures. Therefore, the coupling of these two methods yields an efficient algorithm which can easily handle boundary evolution and takes into account the sensitivity of structures towards small perturbations . Unlike the majority of algorithms for Topology Optimization, the volume constraint is imposed at each iteration by adding a parameter in the level-set function which will enforce it.

The performance and validation of our methodology are evaluated providing several numerical benchmarks and examples showing proper performance and accurate results.

Keywords:
Topology Optimization; Nonlinear Solid Mechanics; Topological Derivative;
Level-set method; Topological Sensitivity Analysis

Contents

List of Figures

List of Tables

Chapter 1

Introduction

1.1 Preface

Usually, considering a linear relation between deformations and stresses suffices to yield valid results, especially in engineering problems. In such cases, a simplification of the General Theory of Elasticity is considered, the so-popular Linear Theory of Elasticity[21]. However, there exist several situations in which this linear relation gives inaccurate results. Sometimes, the material under study presents a nonlinear behavior which translates into a nonlinear relation between strains and stresses. In other situations, displacements are not small enough to neglect their high-order terms. When we are facing these problems, Nonlinear Continuum Mechanics must be applied to ensure a proper description of the solution[5, 6, 22].

The efficient use of materials is clearly an important decision in many different settings. Topology Optimization (TO) is a branch of a group of methods which looks for the optimal design of continuum and discrete structures under a set of boundary conditions and external loads. Unlike other branches, such as size or shape optimization, no prior structural configuration is needed. The optimization of the geometry and topology of structural layouts has widely evolved in the last decades, thanks to a significant number of developments to design complex problems. In fact, structural optimization has been identified as one of the most challenging tasks in structural design.

One of the pioneering methods to deal with the TO problem are the so-called SIMP methods (Solid Isotropic Microstructure with Penalization) [24]. The basis of this approach is to define a density function ρ which indicates the presence $(\rho = 1)$ or absence $(\rho = 0)$ of material within the reference domain. This allows to determine those regions where material must be placed . This material distribution TO technique has been applied to a wide range of different disciplines, such as acoustics, fluid flow, wave propagation, aerospace design and linear and nonlinear elasticity among others [12, 17, 19, 23].

Lately, the introduction of level-set methods in the Computational Mechanics context, was seen as another option to solve the TO problem [3, 10, 15, 27]. This strategy allows to track the interface of the structure in a easier manner. Although the level-set method makes possible topology changes during the optimization process, it does not solve the inherent problem of creating new holes in the middle of a shape. In practice, this basically means that the method is unable to change the interior of the structure and only permits to modify its boundary, which in fact, is the one simulated with the level-set function. As a consequence, this approach seems quite unsuitable to perform the TO analysis on its own.

There exists another family of methods, which studies the variation of some cost function at any point of the domain to determine its sensitivity, being sensitivity understood as how the cost function is affected by changes on it. Such methods are referred in the literature as TSA (Topological Sensitivity Analysis) [1, 7]. The lack of a function to control this sensitivity, motivated the development of the Topological Derivative (TD) [14, 20]. TD emerges as one of the most powerful technique to be applied in TSA methods because it measures the sensitivity of a given functional with respect to an infinitesimal singular perturbation, such as the insertion of holes, expansions or contraction of them and it is derived from mathematical analysis. Therefore, TD can be used as a tool to determine where material has to be removed or added in TSA methods.

The main drawbacks of the already existing codes which deal with TO of Nonlinear Structures with TD as a TSA function is that they need to remove a given quantity of volume per iteration. This procedure is quite rigid because those regions where material is removed are not allowed to be refilled in next iterations. Thus, we are solving a problem in which we are subtracting bit by bit the material until the volume constraint (final percentage of material wanted) is reached. Moreover, elements are not allowed to be refilled even though the TD algorithm points to them .

In this thesis, the concept of TD is applied as a sensitivity function to carry out a TO algorithm in the context of Nonlinear Solid Mechanics. In particular, the assumption of hyperelastic material will be taken into account by considering both Saint Venant-Kirchhoff and Neohookean constitutive models. In addition, a level-set method will be applied coupled with the problem to keep a sharp tracking of the interface. Finally, to fulfill the volume requirement each iteration, a scalar value will be added to the level-set function.

This work is organized as follows. In Chapter 2, the main basis of Nonlinear Continuum mechanics is introduced, emphasizing the main differences with the linear case. In Chapter 3 the constitutive models which allows us to relate the deformation of the structure with the stresses suffered by it will be stated. Especial attention to the isotropic hyperelastic materials is done. Next, Chapter 4 deals with two formulations to discretize the solution of the

Nonlinear Finite Element problem, the Total Lagrangian Formulation and the Updated Lagrangian formulation. The solution methods and time discretization are presented in Chapter 5. In Chapter 6 the topological derivative-based topology optimization of nonlinear structures will be studied. An algorithm will be presented to deal with such problems. To verify our code, some numerical examples are shown in Chapter 7. To end up, several conclusions and future work are drawn in Chapter 8. Finally, some Appendixes can be found to show some mathematical laws (Appendix A) and the well-known Voigt Notation (Appendix B).

1.2 FEMUSS: A Finite Element Code

The Finite Element Method has proven to be an effective method for the spatial approximation of the Topology Optimization of Nonlinear Structures[26]. In this work we plan to implement both the Nonlinear Continuum Mechanics problem and the Topology Optimization one in an in-house code of our research group called `FEMUSS`(Finite Element Method Using Subgrid Scales).

`FEMUSS` is a FEM code written in FORTRAN 2003 [13, 25] which deals with several physics and also coupled problems. It allows parallel implementations, which becomes essential for calculating large quantity of data or working in large scale problems.

In order to solve a problem using `FEMUSS`, we can first define our geometry features using `GiD` preprocessor developed at `CIMNE` (International Center of Numerical Methods in Engineering). After this, all the files generated regarding mesh and conditions will be used by `FEMUSS` to compute the solution of the problem. Finally, the post-processing stage can be done using again `GiD` or any other visualization software such as `Paraview`.

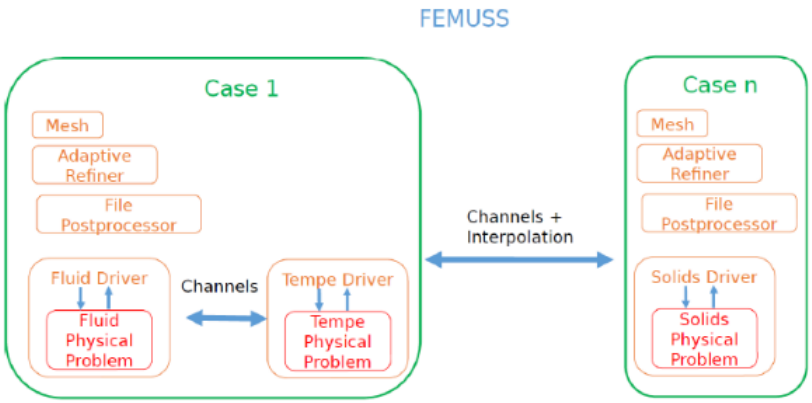

Figure 1.1: General Structure of FEMUSS: Flowchart

The structure of `FEMUSS` is based on hierarchical relations between objects (Figure 1.1).

The main characteristic of this organization is that objects from below in the hierarchy should not 'know' about objects which are above them. This is an important feature of the code, which permits to have a clean programming technique and an agile software development. The higher level structure in FEMUSS are referred as CASES. In each case, all the processes which take place on top of the same mesh are grouped. As a consequence, each case has a MESH, a FILE POSTPROCESSOR and might have several PHYSICAL PROBLEMS. This CASES are defined in such a way that the code is capable of dealing with, for instance, fluid-structure interaction problems, where each of the problems is defined in a different computational domain. The mesh object takes care of all the geometrical information, i.e., elements, connectivities, coordinates, shape functions, etc. We also have the file postprocessor which contains objects in charge of writing information to the disk so that the results can be lately visualized. The final ingredient of this structure is the concept of COMMUNICATION CHANNELS. These are basically a set of pointers which allow to pass information between entities which are on the same hierarchical level.

Chapter 2

Nonlinear Continuum Mechanics

2.1 Introduction

Continuum Mechanics deals with the analysis of the kinematics and the mechanical behavior of materials. In Linear Continuum mechanics an assumption is made that the deformation is sufficiently small to enable the effect of changes in the geometrical configuration of the solid to be ignored, whereas in the Nonlinear case the magnitude of the deformation is unrestricted.

There are two sources of nonlinearity in the analysis of solid continua, namely, material and geometric nonlinearity. The former occurs when the stress-strain behavior given by the constitutive relation is nonlinear. The latter takes into account the effect on the load deformation due to changes in geometry.

Despite the obvious success of the assumption of linearity in engineering analysis it is clear that many situations require consideration of nonlinear behavior. For example, ultimate load analysis of structures involves material and geometric nonlinearity, and any metal-forming analysis must include both of them. Structural instability is inherently a geometric nonlinear phenomenon, as is the behavior of tension structures.

The purpose of this chapter is summarize the Nonlinear Continuum Mechanics that is needed for Nonlinear Finite Element Methods. It begins with a description of deformation and motion. Next, the concepts of stress and strain in Nonlinear Continuum Mechanics are described. Unlike Linear Continuum Mechanics, stress and strain can be defined in many ways in the Nonlinear case. The conservation equations, which are often called balance equations, are described next to end this chapter. In our case, conservation of mass and both linear and angular momentum will be enough to state the problem.

2.2 Deformation and Motion

2.2.1 Motion

Kinematics is the study of motion and deformation without reference to the cause. We shall see immediately that consideration of finite deformation enables alternative coordinate systems to be employed, namely, material and spatial descriptions associated with the names of Lagrange and Euler respectively.

Consider a body in an initial state at a time t=0 as shown in Figure 2.1 ; The domain of the body in the initial state is denoted by Ω_0 and called *the initial configuration*. To describe the motion of the body and deformation, it is also needed a configuration in which various equations are referred, *the reference configuration*. The significance of the reference configuration lies in the fact that motion is defined with respect to this configuration.

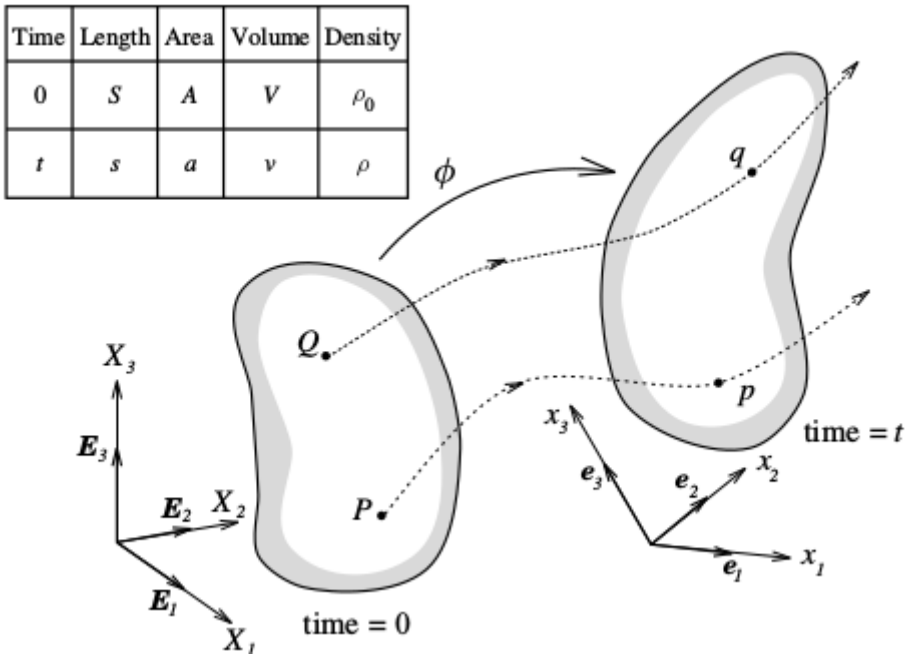

Figure 2.1: General Body Motion of a deformable body. From [6]

The domain of *the current configuration* of the body is denoted by Ω. The boundary of the domain is denoted by Γ. The position vector of a material point in the reference configuration is given by the coordinates $\boldsymbol{X}$. The current positions of these particles are defined by the coordinates $\boldsymbol{x}$, which give the spatial description of the point at time t. The vector variable $\boldsymbol{X}$ for a given material point does not change with time; these variables are called *the material coordinates* or *Lagrangian coordinates.* On the other hand, the variables $\boldsymbol{x}$ are named *the*

spatial or Eulerian coordinates.

The motion can be mathematically described by a mapping ϕ between initial and current particle positions as,

$$\boldsymbol{x} = \phi(\boldsymbol{X}, t) \tag{2.1}$$

There are several mathematical restrictions to ensure the existence of this function and its inverse $\phi^{-1}(\boldsymbol{x}, t)$:

- $\phi(\boldsymbol{X}, 0) = \boldsymbol{X}$, By definition, $\boldsymbol{X}$ is the position of the particles when the motion starts (consistency equation)
- $\phi \in C^1$, the function must be continuous but also its derivatives at any point and for any moment of time.
- ϕ must be a bijective function. Each element of $\boldsymbol{x}$ is paired with exactly one element of the first $\boldsymbol{X}$. Physically, it means that two particles can not occupy simultaneously the same point in the space and one particle can not occupy simultaneously two different points in the space.
- Due to mass conservation (which will be explained later), $\det\left[\frac{\partial \phi(\boldsymbol{X},t)}{\partial \boldsymbol{X}}\right] > 0$. It means that any differential volume must be positive. In addition, it also allows us to say that the density of the particles must be always greater than zero.

2.2.2 Eulerian and Lagrangian Description

Two approaches are used to describe the deformation and response of a continuum. A distinction has to be made between the coordinate systems that can be chosen to describe it. Relevant properties can be described in terms of where the body was before deformation or where it is during it. In the first approach, the material coordinates are considered and it is called the *material or Lagrangian description.* In the second one, spatial coordinates are chosen and it is called the *spatial or Eulerian description.* The duality is similar to that in mesh descriptions. In the development of Lagrangian finite elements, two approaches are commonly taken:

1. Formulations in terms of the Lagrangian measures in which derivatives and integrals are taken with respect to the material coordinates $\boldsymbol{X}$, called *Total Lagrangian formulation.*
2. Formulations expressed in terms of the Eulerian measures in which derivatives and integrals are taken with respect to the spatial coordinates $\boldsymbol{x}$, called *Updated Lagrangian formulation.*

The displacement of a material point is given by the difference between its current position and its original position, so

$$\boldsymbol{u}(\boldsymbol{X},t) = \boldsymbol{x} - \boldsymbol{X} = \phi(\boldsymbol{X},t) - \boldsymbol{X} \tag{2.2}$$

2.2.3 Deformation Gradient

A key quantity in finite deformation analysis is the deformation gradient $\boldsymbol{F}$, which is involved in all equations relating quantities before deformation to corresponding quantities after deformation. The deformation gradient is defined by,

$$\boldsymbol{F} = \frac{\partial \boldsymbol{x}}{\partial \boldsymbol{X}} \text{ or } F_{ij} = \frac{\partial x_i}{\partial X_j} \tag{2.3}$$

The determinant of $\boldsymbol{F}$ is denoted by J and called the *Jacobian determinant* or the determinant of the deformation gradient

$$J = \det(\boldsymbol{F}) = \det\left[\frac{\partial \phi(\boldsymbol{X},t)}{\partial \boldsymbol{X}}\right] \tag{2.4}$$

The Jacobian determinant gives the volume change as,

$$dv = J \cdot dV \tag{2.5}$$

It is also advisable to define the deformation gradient in terms of the displacement field,

$$\boldsymbol{F} = \frac{\partial \boldsymbol{x}}{\partial \boldsymbol{X}} = \frac{\partial(\boldsymbol{u}+\boldsymbol{X})}{\partial \boldsymbol{X}} = \frac{\partial \boldsymbol{u}}{\partial \boldsymbol{X}} + \frac{\partial \boldsymbol{X}}{\partial \boldsymbol{X}} = \nabla_0 \boldsymbol{u} + \boldsymbol{I} \tag{2.6}$$

where $\nabla_0 \boldsymbol{u}$ is the material gradient of the displacement field and I the identity matrix.

2.3 Strain Measures

In contrast to Linear Elasticity, many different measures of strain are used in Nonlinear Continuum Mechanics.

2.3.1 Right and Left Cauchy-Green Deformation Tensors

The Right Cauchy-Green Deformation Tensor $\boldsymbol{C}$ is defined as,

$$\boldsymbol{C} = \boldsymbol{F}^T \boldsymbol{F} \tag{2.7}$$

It allows us to find the spatial scalar product $d\boldsymbol{x}_1 \cdot d\boldsymbol{x}_2$ in terms of the material vectors $d\boldsymbol{X}_1$ and $d\boldsymbol{X}_2$ as,

$$d\boldsymbol{x}_1 \cdot d\boldsymbol{x}_2 = d\boldsymbol{X}_1 \cdot \boldsymbol{C} \cdot d\boldsymbol{X}_2 \tag{2.8}$$

Alternatively the initial material scalar product $d\boldsymbol{X}_1 \cdot d\boldsymbol{X}_2$ can be obtained in terms of the spatial vectors $d\boldsymbol{x}_1$ and $d\boldsymbol{x}_2$ via the Left Cauchy-Green Deformation Tensor $\boldsymbol{b}$,

$$\boldsymbol{b} = \boldsymbol{F}\boldsymbol{F}^T \qquad \Rightarrow d\boldsymbol{X}_1 \cdot d\boldsymbol{X}_2 = d\boldsymbol{x}_1 \cdot \boldsymbol{b}^{-1} \cdot d\boldsymbol{x}_2 \tag{2.9}$$

2.3.2 Green-Lagrange and Almansi Strain Tensors

The Green-Lagrange Strain Tensor $\boldsymbol{E}$ is defined by

$$ds^2 - dS^2 = 2d\boldsymbol{X} \cdot \boldsymbol{E} \cdot d\boldsymbol{X} \qquad \Rightarrow \boldsymbol{E} = \frac{1}{2}(\boldsymbol{C} - \boldsymbol{I}) \tag{2.10}$$

so it gives the change in the square of the length of the material vector $d\boldsymbol{X}$. The Green Strain Tensor can also be expressed in terms of displacement gradients by

$$E_{ij} = \frac{1}{2}\left(\frac{\partial u_i}{\partial X_j} + \frac{\partial u_j}{\partial X_i} + \frac{\partial u_k}{\partial X_i}\frac{\partial u_k}{\partial X_j}\right) \tag{2.11}$$

The same change can be expressed with reference to the spatial elemental vector $d\boldsymbol{x}$ thanks to the Almansi Strain Tensor $\boldsymbol{e}$,

$$ds^2 - dS^2 = 2d\boldsymbol{x} \cdot \boldsymbol{e} \cdot d\boldsymbol{x} \qquad \Rightarrow \boldsymbol{e} = \frac{1}{2}(\boldsymbol{I} - \boldsymbol{b}^{-1}) \tag{2.12}$$

It can also be expressed in terms of displacement gradients,

$$e_{ij} = \frac{1}{2}\left(\frac{\partial u_i}{\partial x_j} + \frac{\partial u_j}{\partial x_i} - \frac{\partial u_k}{\partial x_i}\frac{\partial u_k}{\partial x_j}\right) \tag{2.13}$$

It is easy to check, that both tensors matches in the Engineering Strain tensor $\boldsymbol{\varepsilon}$ in the Infinitesimal Strain Theory, where the displacements and their gradients are small enough to neglect second order terms and the material and spatial coordinates are considered similar $\boldsymbol{x} \approx \boldsymbol{X}$,

$$\varepsilon_{ij} = e_{ij} = E_{ij} = \frac{1}{2}\left(\frac{\partial u_i}{\partial X_j} + \frac{\partial u_j}{\partial X_i}\right) \tag{2.14}$$

2.4 Stress Measures

In Nonlinear problems, several stress measures can be defined. We will consider three measures of stress:

1. The Cauchy stress, $\boldsymbol{\sigma}$
2. The First Piola-Kirchhoff stress, $\boldsymbol{P}$
3. The Second Piola-Kirchhoff stress, $\boldsymbol{S}$

While both $\boldsymbol{S}$ and $\boldsymbol{P}$ are defined in the reference configuration, $\boldsymbol{\sigma}$ is defined in the current configuration. The stresses are defined by Cauchy's law

$$\boldsymbol{n}\cdot\boldsymbol{\sigma}d\Gamma = \boldsymbol{t}d\Gamma \qquad \Leftrightarrow \qquad \boldsymbol{n}_0\cdot\boldsymbol{P}d\Gamma_0 = \boldsymbol{t}_0 d\Gamma_0 \qquad \Leftrightarrow \qquad \boldsymbol{n}_0\cdot\boldsymbol{S}d\Gamma_0 = \boldsymbol{F}^{-1}\boldsymbol{t}_0 d\Gamma_0 \tag{2.15}$$

where $\boldsymbol{t}$ is the traction in the current configuration and $\boldsymbol{t}_0$ in the reference one. See Figure 2.2 to further details.

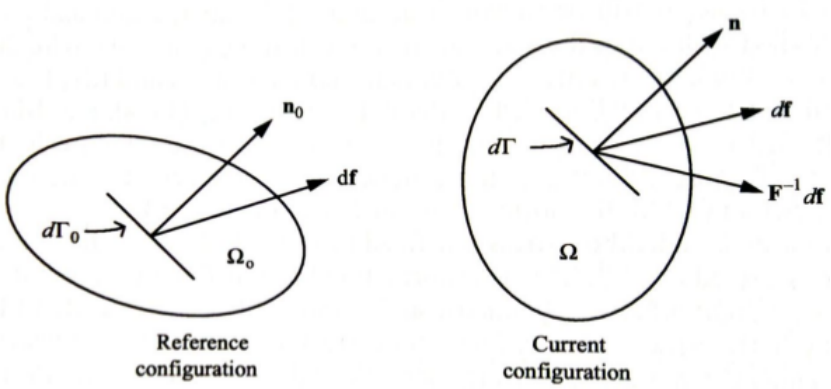

Figure 2.2: Definition of Stress measures. From [5]

It can be interesting to look for the transformation between stresses. They are interrelated by functions of the deformation

$$\boldsymbol{P} = J\boldsymbol{F}^{-1}\cdot\boldsymbol{\sigma} \tag{2.16}$$

$$\boldsymbol{\sigma} = J^{-1}\boldsymbol{F}\cdot\boldsymbol{S}\cdot\boldsymbol{F}^{T} \tag{2.17}$$

$$\boldsymbol{P} = \boldsymbol{S}\cdot\boldsymbol{F}^{T} \tag{2.18}$$

The above relations between the Piola-Kirchhoff stresses and the Cauchy stress depend only upon the deformation gradient $\boldsymbol{F}$ and the Jacobian determinant J. Thus, if the deformation is known, the state of stress can always be expressed in terms of any stress tensor.

2.5 Conservation Equations

One group of fundamental equations of Continuum Mechanics arises from the conservation laws. These equations must always be satisfied by physical systems. Let us enumerate them and explain the consequence of their conservation.

2.5.1 Conservation of mass

Mass $m(\Omega)$ of a material domain Ω is given by

$$m(\Omega) = \int_{\Omega} \rho(\boldsymbol{X},t) d\Omega \tag{2.19}$$

where $\rho(\boldsymbol{X},t)$ is the density. Mass conservation requires that the mass of any material domain be constant, since no material flows through the boundaries of a material domain. Therefore, the material time derivative of $m(\Omega)$ vanishes,

$$\frac{Dm}{Dt} = \frac{D}{Dt}\int_{\Omega} \rho d\Omega = \int_{\Omega} \left(\frac{D\rho}{Dt} + \rho \nabla \cdot \boldsymbol{v} \right) d\Omega = 0 \tag{2.20}$$

where the last equality comes from the Reynold's transport theorem, (Appendix A.2). Since the above equation holds for any subdomain Ω, it follows that

$$\frac{D\rho}{Dt} + \rho \nabla \cdot \boldsymbol{v} = 0 \tag{2.21}$$

When a material is incompressible, the material time derivative of the density vanishes, and it can be seen from Equation 2.21 that the mass conservation equation becomes

$$\nabla \cdot \boldsymbol{v} = 0 \tag{2.22}$$

For Lagrangian descriptions, the mass conservation can be integrated in time to obtain an algebraic equation for the density

$$\int_{\Omega} \rho d\Omega = \int_{\Omega_0} \rho_0 d\Omega_0 \tag{2.23}$$

and taking into account that the Jacobian allows us to relate volume changes, then

$$\int_{\Omega} \rho d\Omega = \int_{\Omega_0} \rho J d\Omega_0 = \int_{\Omega_0} \rho_0 d\Omega_0 \quad \Leftrightarrow \quad \int_{\Omega_0} (\rho J - \rho_0)\, d\Omega_0 = 0 \tag{2.24}$$

Invoking the smoothness of the integrand, the equation for mass conservation in Lagrangian formulation yields

$$\rho(\boldsymbol{X},t) \cdot J(\boldsymbol{X},t) = \rho_0(\boldsymbol{X}) \tag{2.25}$$

2.5.2 Conservation of linear momentum

The equation emanating from the principle of linear momentum is a key equation in Nonlinear Finite Element procedures. Linear momentum conservation is equivalent to Newton's Second law of motion, which relates the forces acting on a body to its acceleration. We consider an arbitrary domain Ω with boundary Γ subjected to a body force $\rho\boldsymbol{b}$ and to a surface traction $\boldsymbol{t}$, where $\boldsymbol{b}$ is a force per unit mass and $\boldsymbol{t}$ is a force per unit area. The total force is given by

$$\boldsymbol{f}(t) = \int_{\Omega} \rho \boldsymbol{b}(\boldsymbol{x},t) d\Omega + \int_{\Gamma} \boldsymbol{t}(\boldsymbol{x},t) d\Gamma \tag{2.26}$$

The linear momentum is given by

$$\boldsymbol{p}(t) = \int_{\Omega} \rho \boldsymbol{v}(\boldsymbol{x},t) d\Omega \tag{2.27}$$

where $\rho\boldsymbol{v}$ is the linear momentum per unit volume.

Newton's second law of motion states that the material time derivative of the linear momentum equals the total force.

$$\frac{D\boldsymbol{p}}{Dt} = \boldsymbol{f} \quad \Leftrightarrow \quad \frac{D}{Dt}\int_{\Omega} \rho \boldsymbol{v}(\boldsymbol{x},t) d\Omega = \int_{\Omega} \rho \boldsymbol{b}(\boldsymbol{x},t) d\Omega + \int_{\Gamma} \boldsymbol{t}(\boldsymbol{x},t) d\Gamma \tag{2.28}$$

Now we can apply Reynold's transport theorem (Appendix A.2) to the first integrand to obtain

$$\frac{D}{Dt}\int_{\Omega} \rho \boldsymbol{v} d\Omega = \int_{\Omega} \left(\frac{D}{Dt}(\rho \boldsymbol{v}) + \text{ div } (\boldsymbol{v}) \rho \boldsymbol{v} \right) d\Omega = \int_{\Omega} \left[\rho \frac{D\boldsymbol{v}}{Dt} + \boldsymbol{v} \left(\frac{D\rho}{Dt} + \rho \text{ div } (\boldsymbol{v}) \right) \right] d\Omega \tag{2.29}$$

where the chain rule has been applied in the last equality. Taking into account the mass

conservation equation 2.21, the term multiplying the velocity vanishes, giving

$$\frac{D}{Dt}\int_{\Omega}\rho\boldsymbol{v}d\Omega=\int_{\Omega}\rho\frac{D\boldsymbol{v}}{Dt}d\Omega \tag{2.30}$$

On the other hand, we can use Cauchy's relation between the Cauchy stress $\boldsymbol{\sigma}$ and traction $\boldsymbol{t}$ in the third integrand for the conservation of linear momentum

$$\int_{\Gamma}\boldsymbol{t}d\Gamma=\int_{\Gamma}\boldsymbol{n}\cdot\boldsymbol{\sigma}d\Gamma=\int_{\Omega}\nabla\cdot\boldsymbol{\sigma}d\Omega \tag{2.31}$$

where the last equality comes from the Gauss's theorem (Appendix A.1). Substituting (Equation 2.30) and (Equation 2.31) into the conservation of linear momentum (Equation 2.28) it gives

$$\int_{\Omega}\left(\rho\frac{D\boldsymbol{v}}{Dt}-\rho\boldsymbol{b}-\nabla\cdot\boldsymbol{\sigma}\right)d\Omega=0 \tag{2.32}$$

Since this equation holds for an arbitrary domain Ω,

$$\rho\boldsymbol{a}=\rho\boldsymbol{b}+\nabla\cdot\boldsymbol{\sigma} \tag{2.33}$$

where $\boldsymbol{a}=\frac{D\boldsymbol{v}}{Dt}$ is the material derivative of the velocity field, that is the acceleration of the system.

When loads are applied slowly and the inertial forces are very small and can be neglected then acceleration can be dropped from Equation 2.33 to obtain the so-called *Equilibrium equation*

$$\rho\boldsymbol{b}+\nabla\cdot\boldsymbol{\sigma}=0 \tag{2.34}$$

Problems in which equilibrium equation can be applied are often called static problems.

2.5.3 Conservation of angular momentum

By taking the cross-product of each term in the corresponding linear momentum principle, the integral form of the conservation of angular momentum is obtained

$$\frac{D}{Dt}\int_{\Omega}\boldsymbol{x}\times\rho\boldsymbol{v}(\boldsymbol{x},t)d\Omega=\int_{\Omega}\boldsymbol{x}\times\rho\boldsymbol{b}(\boldsymbol{x},t)d\Omega+\int_{\Gamma}\boldsymbol{x}\times\boldsymbol{t}(\boldsymbol{x},t)d\Gamma \tag{2.35}$$

After some manipulations, the condition which follows from this equation yields,

$$\boldsymbol{\sigma} = \boldsymbol{\sigma}^T \tag{2.36}$$

In other words, conservation of angular momentum requires that the Cauchy stress be a symmetric tensor. Taking into account the transformations between stresses (Equations 2.17),

$$\boldsymbol{\sigma} = \boldsymbol{\sigma}^T \;\Leftrightarrow\; J^{-1}\boldsymbol{F}\cdot\boldsymbol{S}\cdot\boldsymbol{F}^T = \left(J^{-1}\boldsymbol{F}\cdot\boldsymbol{S}\cdot\boldsymbol{F}^T\right)^T \;\Leftrightarrow\; J^{-1}\boldsymbol{F}\cdot\boldsymbol{S}\cdot\boldsymbol{F}^T = J^{-1}\cdot\left(\boldsymbol{F}^T\right)^T\cdot\left(\boldsymbol{F}\cdot\boldsymbol{S}\right)^T \;\Leftrightarrow$$

$$\Leftrightarrow \boldsymbol{F}\cdot\boldsymbol{S}\cdot\boldsymbol{F}^T = \boldsymbol{F}\cdot\boldsymbol{S}^T\cdot\boldsymbol{F}^T \;\Leftrightarrow\; \boldsymbol{S} = \boldsymbol{S}^T \tag{2.37}$$

which implies that the Second Piola-Kirchhoff stress tensor $\boldsymbol{S}$ must be also symmetric. However, regarding to the First Piola-Kirchhoff stress $\boldsymbol{P}$

$$\boldsymbol{S} = \boldsymbol{S}^T \;\Leftrightarrow\; \boldsymbol{P}\cdot\boldsymbol{F}^{-T} = \left(\boldsymbol{P}\cdot\boldsymbol{F}^{-T}\right)^T \;\Leftrightarrow\; \boldsymbol{P}\cdot\boldsymbol{F}^{-T} = \left(\boldsymbol{F}^{-T}\right)^T\cdot\boldsymbol{P}^T \;\Leftrightarrow\; \boldsymbol{P}\cdot\boldsymbol{F}^T = \boldsymbol{F}\cdot\boldsymbol{P}^T \tag{2.38}$$

which means that conservation of angular momentum does not require that the First Piola-Kirchhoff stress tensor $\boldsymbol{P}$ be a symmetric tensor. For this reason, in Nonlinear Computational Mechanics is widely used the Second one.

Chapter 3

Constitutive Model

3.1 Introduction

The response of the material is characterized by a constitutive equation which expresses the stress in terms of some measure of the deformation history. These relationships obviously depend upon the type of material under consideration and may be either dependent upon or independent of time.

Generally, constitutive equations must satisfy certain physical principles. In this chapter the constitutive equations will be established in the context of a hyperelastic material, whereby stresses are derived from a stored elastic energy function. Particularly, two models will be introduced: The Saint Venant-Kirchhoff Material and Neo-Hookean Material.

3.2 HyperElasticity

Materials for which work is independent of the load path are said to be *hyperelastic* materials. These materials are said to satisfy automatically the second law of Thermodynamics. Let us state the local form of the second law of Thermodynamics through the Clausius-Duhem inequality

$$\Xi = -\dot{\psi} - \eta\,\dot{\theta} + \boldsymbol{S} : \dot{\boldsymbol{E}} - \frac{1}{\theta}\boldsymbol{q}_0 \cdot \nabla\theta \geq 0 \tag{3.1}$$

where ψ is the internal specific energy or strain energy function, η is the specific entropy, $\boldsymbol{q}_0$ is the heat flux vector, θ the temperature and Ξ is the dissipation of the system. This expression states that the dissipation of the system must be always greater than or equal to zero. Considering purely deformative processes where temperature and entropy remain constant, equation 3.1 yields

$$\Xi = -\dot{\psi} + \boldsymbol{S} : \dot{\boldsymbol{E}} \geq 0 \tag{3.2}$$

Taking into account that hyperelastic materials are considered with a reversible character in their loading process, the dissipation of the system must be null.

$$\Xi = -\dot{\psi} + \boldsymbol{S} : \dot{\boldsymbol{E}} = 0 \quad \Leftrightarrow \quad \dot{\psi} = \boldsymbol{S} : \dot{\boldsymbol{E}} \tag{3.3}$$

The material derivative of the stored energy function is defined as

$$\dot{\psi} = \frac{\partial \psi(\boldsymbol{E})}{\partial \boldsymbol{E}} : \frac{\partial \boldsymbol{E}}{\partial t} \tag{3.4}$$

Thus,

$$\dot{\psi} = \boldsymbol{S} : \dot{\boldsymbol{E}} = \boldsymbol{S} : \frac{\partial \boldsymbol{E}}{\partial t} = \frac{\partial \psi(\boldsymbol{E})}{\partial \boldsymbol{E}} : \frac{\partial \boldsymbol{E}}{\partial t} \quad \Leftrightarrow \quad \boldsymbol{S} = \frac{\partial \psi(\boldsymbol{E})}{\partial \boldsymbol{E}} \tag{3.5}$$

This procedure allows us to state that, given a material of which stresses can be defined through a stored energy function satisfying equation 3.5 and considering purely deformative processes, the second law of Thermodynamics will be automatically satisfied. These materials can be characterized also with the Right-Cauchy tensor $\boldsymbol{C}$:

$$\boldsymbol{S} = 2\frac{\partial \psi(\boldsymbol{C})}{\partial \boldsymbol{C}} = \frac{\partial \hat{\psi}(\boldsymbol{E})}{\partial \boldsymbol{E}} \tag{3.6}$$

Note that potential can be expressed as a function of either the Right Cauchy-Green Deformation Tensor $\boldsymbol{C}$ or the Green strain $\boldsymbol{E}$. A consequence of the existence of a stored energy function is that the work done on a hyperelastic material is independent of the deformation path.

The relationship between $\boldsymbol{S}$ and either $\boldsymbol{E}$ or $\boldsymbol{C}$ given by equation 3.6 will invariably be nonlinear. Within the framework of a Newton-Raphson solution , the relationship will need to be linearized. The relationship between the directional derivatives of $\boldsymbol{S}$ and $\boldsymbol{E}$ is expressed as:

$$\dot{\boldsymbol{S}} = \mathbb{C} : \dot{\boldsymbol{E}} \tag{3.7}$$

where $\mathbb{C}$ is the tangent modulus known as *the Lagrangian or material elasticity tensor*. It can be obtained from the stored energy function ψ,

$$\mathbb{C} = \frac{\partial \boldsymbol{S}}{\partial \boldsymbol{E}} = 2\frac{\partial \boldsymbol{S}}{\partial \boldsymbol{C}} = 4\frac{\partial^2 \psi}{\partial \boldsymbol{C} \partial \boldsymbol{C}} \tag{3.8}$$

Recalling that the Deformation power in a material subdomain can be defined through the

work conjugates,

$$W^D = \int_{\Omega} \boldsymbol{\sigma} : \boldsymbol{d} d\Omega = \int_{\Omega_0} \boldsymbol{P} : \dot{\boldsymbol{F}} d\Omega_0 = \int_{\Omega_0} \boldsymbol{S} : \frac{1}{2}\dot{\boldsymbol{C}} d\Omega_0 \tag{3.9}$$

and by replacing Equation 3.8 on it,

$$W^D(t) = \oint \boldsymbol{S} : \frac{1}{2}\dot{\boldsymbol{C}} dt = \oint 2\frac{\partial \psi(\boldsymbol{C})}{\partial \boldsymbol{C}} : \frac{1}{2}\dot{\boldsymbol{C}} dt = \oint \frac{\partial \psi(\boldsymbol{C})}{\partial \boldsymbol{C}} : \dot{\boldsymbol{C}} dt = 0 \tag{3.10}$$

Therefore, the existence of this stored energy function implies that our model is thermodynamically consistent and there is no necessity in checking it.

3.2.1 Isotropic HyperElastic Materials

Isotropy is defined by requiring the constitutive behavior to be identical in any material direction. This implies that the relationship between the stored energy function ψ and $\boldsymbol{C}$ must be independent of the material axes chosen and, consequently, ψ must only be a function of the invariants of $\boldsymbol{C}$ as,

$$\psi(\boldsymbol{C}(\boldsymbol{X}), \boldsymbol{X}) = \psi(I_{\boldsymbol{C}}, II_{\boldsymbol{C}}, III_{\boldsymbol{C}}, \boldsymbol{X}) \tag{3.11}$$

where the invariants of $\boldsymbol{C}$ are defined here as,

$$\begin{aligned} I_{\boldsymbol{C}} &= \text{trace}\, \boldsymbol{C} = C_{ii} \\ II_{\boldsymbol{C}} &= \frac{1}{2}\left\{ (\text{trace}\,(\boldsymbol{C}))^2 - \text{trace}\left(\boldsymbol{C}^2\right) \right\} = \frac{1}{2}\left\{ (C_{ii})^2 - C_{ij}C_{ji} \right\} \\ III_{\boldsymbol{C}} &= \det \boldsymbol{C} = J^2 \end{aligned} \tag{3.12}$$

3.2.1.1 Saint Venant-Kirchhoff Material

Many engineering applications involve small strains and large rotations. In these problems the effects of large deformation are primarily due to rotations. The response of the material may then be modeled by a simple extension of the linear elastic laws by replacing the Cauchy stress $\boldsymbol{\sigma}$ by the Second Piola-Kirchhoff stress $\boldsymbol{S}$ and the engineering strain $\boldsymbol{\varepsilon}$ by the Green strain $\boldsymbol{E}$.

Therefore, the tensor $\mathbb{C}$ is defined as,

$$\mathbb{C}_{ijkl} = \lambda \delta_{ij}\delta_{kl} + \mu\left(\delta_{ik}\delta_{jl} + \delta_{il}\delta_{jk}\right), \quad \mathbb{C} = \lambda \boldsymbol{I} \otimes \boldsymbol{I} + 2\mu \boldsymbol{I} \tag{3.13}$$

where λ and μ are the Lamé constants. The stress-strain relation for an isotropic Kirchhoff

material may therefore be written as

$$S_{ij} = \lambda E_{kk}\delta_{ij} + 2\mu E_{ij} = \mathbb{C}_{ijkl} \cdot E_{kl}, \quad \boldsymbol{S} = \lambda \text{ trace}(\boldsymbol{E})\boldsymbol{I} + 2\mu\boldsymbol{E} \tag{3.14}$$

Recall that the Lamé constants can be expressed in terms of other constant which are more closely related to physical measurements, the bulk modulus K, Young's modulus E and Poisson's ratio ν , by

$$\mu = \frac{E}{2(1+\nu)}, \quad \lambda = \frac{\nu E}{(1+\nu)(1-2\nu)}, \quad K = \lambda + \frac{2\mu}{3} \tag{3.15}$$

This material is quite easy to be implemented. However, it presents several inconsistencies. On the one hand, in large strains deformation the model becomes useless. On the other hand, it does not satisfy the so-called *growth conditions*. Growth conditions check that the stored energy function of the model goes to infinity when the Jacobian goes to 0. Physically, it means that, as it is impossible to obtain $J = 0$ because it would imply that the domain has been removed, the energy needed to do such a process would be infinity. For these inconsistencies among others, this model is not applied normally in NonLinear Computational Mechanics when large strains are involved.

3.2.1.2 Neo-Hookean Material

The Neo-Hookean material model is an extension of the isotropic linear law (Hooke's law) to large deformation. This material exhibits characteristics that can be identified with the familiar material parameters found in Linear Elastic analysis. The stored energy function for a compressible Neo-Hookean material is

$$\psi(\boldsymbol{C}) = \frac{1}{2}\lambda (\ln J)^2 - \mu \ln J + \frac{1}{2}\mu (\text{ trace } \boldsymbol{C} - \text{ trace } \boldsymbol{I}) \tag{3.16}$$

From Equation 3.6, the stresses are given by differentiating the stored energy function with respect to the Right Cauchy tensor,

$$S_{ij} = \lambda \ln J C^{-1}_{ij} + \mu \left(\delta_{ij} - C^{-1}_{ij}\right), \quad \boldsymbol{S} = \lambda \ln J \boldsymbol{C}^{-1} + \mu \left(\boldsymbol{I} - \boldsymbol{C}^{-1}\right) \tag{3.17}$$

Letting $\lambda' = \lambda$ and $\mu' = \mu - \lambda \ln J$ and using equation 3.8, the elasticity tensor (tangent moduli) yields, in component form,

$$\mathbb{C}_{ijkl} = \lambda' C^{-1}_{ij} C^{-1}_{kl} + \mu' \left(C^{-1}_{ik} C^{-1}_{jl} + C^{-1}_{il} C^{-1}_{kj}\right)$$

To end this chapter, it is easy to verify that this model satisfies the growth conditions before explained. When $J \to 0$, then $\ln J \to \infty$ and therefore $\psi(\boldsymbol{C}) \to \infty$.

Chapter 4

Lagrangian Finite Elements Discretization

4.1 Introduction

In Lagrangian meshes, both nodes and elements move with the material. Boundaries and interfaces remain coincident with element edges, so that their treatment is simplified. Constitutive equations are always evaluated in the same quadrature points. For these reasons, Lagrangian meshes are widely used for Solid Mechanics.

Finite Element discretizations with Lagrangian meshes are commonly classified as *Updated Lagrangian formulations* and *Total Lagrangian formulations* . This chapter begins stating the Updated Lagrangian formulation. The momentum equation is discretized and expressed in terms of the spatial coordinates and the Cauchy stress $\boldsymbol{\sigma}$. The principle of virtual work will be stated which is the weak form of the momentum equation.

The Total Lagrangian formulation is shown next. In this formulation, the Second Piola Kirchhoff stress $\boldsymbol{S}$ is used. As a measure of strain we will use the Green strain tensor $\boldsymbol{E}$ which is the work conjugate of $\boldsymbol{S}$. Also the principle of virtual work will be stated for this formulation.

It is not the goal of this chapter to develop all the process behind the final formulations. We refer to [5, 6] for more details on the formulation.

4.2 Updated Lagrangian Formulation

First of all, we state the principle of virtual work which is the weak form of the momentum Equation 2.33,

$$\int_{\Omega} \delta v_i \rho \ddot{u}_i d\Omega + \int_{\Omega} \frac{\partial (\delta v_i)}{\partial x_j} \sigma_{ji} d\Omega = \int_{\Omega} \delta v_i \rho b_i d\Omega + \int_{\Gamma_N} \delta v_i t_i \tag{4.1}$$

where δv_i is a test function such that $\delta v_i \in \mathscr{V}_0$,

$$\mathscr{V}_0 = \left\{ \delta v_i \mid \delta v_i \in C^0(\boldsymbol{X}), \delta v_i = 0 \text{ on } \Gamma_D \right\} \tag{4.2}$$

where Γ_D is the Dirichlet part of the boundary, where displacements are prescribed and Γ_N the Neumann part of the boundary, where tractions are prescribed. On the other hand, the displacement trial functions u_i live in the space given by

$$u_i \in \mathscr{U}, \quad \mathscr{U} = \left\{ u_i \mid u_i \in C^0(\boldsymbol{X}), u_i = \overline{u_i} \text{ on } \Gamma_D \right\} \tag{4.3}$$

The current domain $\boldsymbol{\Omega}$ is subdivided into elements Ω_e so that the union of the elements comprises the total domain, $\Omega = \bigcup \Omega_e$. The nodal coordinates in the current configuration are denoted by $x_{iI}, I = 1 \text{to } n_n$. Lower case subscripts are used for components, upper case subscripts for nodal values. The nodal coordinates in the undeformed configuration are X_{iI}.

The motion $\boldsymbol{x}(\boldsymbol{X},t)$ is approximated by,

$$x_i(\boldsymbol{X},t) = N_I(\boldsymbol{X}) x_{iI}(t) \tag{4.4}$$

where $N_I(\boldsymbol{X})$ are the shape functions and $x_{iI}(t)$ are the nodal values of the node I. In a Lagrangian mesh, nodes remain coincident with the material points.

Displacement field is defined as,

$$u_i(\boldsymbol{X},t) = x_i(\boldsymbol{X},t) - X_i = u_{iI}(t) N_I(\boldsymbol{X}) \tag{4.5}$$

where $u_{iI}(t)$ are the nodal displacements. The discrete form of the principle of virtual work yields,

$$\underbrace{\int_{\Omega} \frac{\partial (N_I)}{\partial x_j} \sigma_{ji} d\Omega}_{\boldsymbol{f}_{\text{int}}} + \underbrace{\int_{\Omega} N_I \rho \ddot{u}_i d\Omega}_{\boldsymbol{Ma}} = \underbrace{\int_{\Omega} N_I \rho b_i d\Omega + \int_{\Gamma_N} N_I t_i d\Gamma}_{\boldsymbol{f}_{\text{ext}}} \tag{4.6}$$

For a better physical interpretation, it is worthwhile to define each term in the above equation.

The Mass matrix is defined as:

$$M_{ijIJ} = \delta_{ij} \int_{\Omega} \rho N_I N_J d\Omega \tag{4.7}$$

and accelerations are obtained by taking the second material time derivative of the displacements, giving

$$\ddot{u}_i(\boldsymbol{X},t) = \ddot{u}_{iI}(t) N_I(\boldsymbol{X}) \tag{4.8}$$

Defining the $\boldsymbol{B}_I$ matrix associated with the node I such that

$$\boldsymbol{B}_I = \begin{bmatrix} \frac{\partial N_I}{\partial x} & 0 \\ 0 & \frac{\partial N_I}{\partial y} \\ \frac{\partial N_I}{\partial y} & \frac{\partial N_I}{\partial x} \end{bmatrix} \text{ in 2D and } \boldsymbol{B}_I = \begin{bmatrix} \frac{\partial N_I}{\partial x} & 0 & 0 \\ 0 & \frac{\partial N_I}{\partial y} & 0 \\ 0 & 0 & \frac{\partial N_I}{\partial z} \\ \frac{\partial N_I}{\partial y} & \frac{\partial N_I}{\partial x} & 0 \\ \frac{\partial N_I}{\partial z} & 0 & \frac{\partial N_I}{\partial x} \\ 0 & \frac{\partial N_I}{\partial z} & \frac{\partial N_I}{\partial y} \end{bmatrix} \text{ in 3D} \tag{4.9}$$

The $\boldsymbol{B}$ matrix is defined as

$$\boldsymbol{B} = \begin{bmatrix} \boldsymbol{B}_1 & \boldsymbol{B}_2 & \boldsymbol{B}_3 & \cdots & \boldsymbol{B}_m \end{bmatrix} \text{ where m is the number of nodes in that element.}$$

We are able to define the Internal nodal forces in Voigt Notation(Appendix B) as:

$$\boldsymbol{f}_I^{\text{int}} = \int_{\Omega} \frac{\partial (N_I)}{\partial x_j} \sigma_{ji} d\Omega = \int_{\Omega} \boldsymbol{B}_I^T \{\boldsymbol{\sigma}\} d\Omega \tag{4.10}$$

4.3 Total Lagrangian Formulation

First of all, we state the principle of virtual work which is the weak form of the momentum equation 2.33,

$$\underbrace{\int_{\Omega_0} \delta u_i \rho_0 \ddot{u}_i d\Omega_0}_{M\boldsymbol{a}} + \underbrace{\int_{\Omega_0} \partial F_{ij} P_{ji} d\Omega_0}_{\boldsymbol{f}_{\text{int}}} = \underbrace{\int_{\Omega_0} \delta u_i \rho_0 b_i d\Omega_0 + \int_{\Gamma^0{}_N} \delta u_i t^0{}_i d\Gamma}_{\boldsymbol{f}_{\text{ext}}} \tag{4.11}$$

where $\delta u_i$is the test function such that $\delta u_i \in \mathscr{U}_0$,

$$\mathscr{U}_0 = \left\{ \delta u_i \mid \delta u_i \in C^0(\boldsymbol{X}), \delta u_i = 0 \text{ on } \Gamma_D \right\} \tag{4.12}$$

and $u_i \in \mathscr{U}$ the displacement trial functions.

We define a Lagrangian mesh with the same properties as described in Section 4.2. To define the Internal nodal forces in Voigt Notation it is of little use to write the nodal forces in terms of $\boldsymbol{P}$ since it is not symmetric. Therefore, we will write the internal force term in terms of the Second Piola-Kirchhoff stress $\boldsymbol{S}$. Using the transformation $\boldsymbol{P} = \boldsymbol{S} \cdot \boldsymbol{F}^T$, the expression for the internal forces becomes

$$f_{jI}^{\text{int}} = \int_{\Omega_0} \partial F_{ij} P_{ji} d\Omega_0 = \int_{\Omega_0} \frac{\partial N_I}{\partial X_j} F_{jk} S_{ik} d\Omega_0 \tag{4.13}$$

Defining a $\boldsymbol{B}_0$ matrix such that

$$B^0_{\text{ikjI}} = \underset{\text{(i,k)}}{\text{sym}} \left(\frac{\partial N_I}{\partial X_i} F_{jk} \right) \tag{4.14}$$

The $\boldsymbol{B}_I^0$ matrix associated to the node I yields,

$$\boldsymbol{B}_I^0 = \begin{bmatrix} \frac{\partial N_I}{\partial X}\frac{\partial x}{\partial X} & \frac{\partial N_I}{\partial X}\frac{\partial y}{\partial X} \\ \frac{\partial N_I}{\partial Y}\frac{\partial x}{\partial Y} & \frac{\partial N_I}{\partial Y}\frac{\partial y}{\partial Y} \\ \frac{\partial N_I}{\partial X}\frac{\partial x}{\partial Y} + \frac{\partial N_I}{\partial Y}\frac{\partial x}{\partial X} & \frac{\partial N_I}{\partial X}\frac{\partial y}{\partial Y} + \frac{\partial N_I}{\partial Y}\frac{\partial y}{\partial X} \end{bmatrix} \text{ in 2D} \tag{4.15}$$

and

$$\boldsymbol{B}_I^0 = \begin{bmatrix} \frac{\partial N_I}{\partial X}\frac{\partial x}{\partial X} & \frac{\partial N_I}{\partial X}\frac{\partial y}{\partial X} & \frac{\partial N_I}{\partial X}\frac{\partial z}{\partial X} \\ \frac{\partial N_I}{\partial Y}\frac{\partial x}{\partial Y} & \frac{\partial N_I}{\partial Y}\frac{\partial y}{\partial Y} & \frac{\partial N_I}{\partial Y}\frac{\partial z}{\partial Y} \\ \frac{\partial N_I}{\partial Z}\frac{\partial x}{\partial Z} & \frac{\partial N_I}{\partial Z}\frac{\partial y}{\partial Z} & \frac{\partial N_I}{\partial Z}\frac{\partial z}{\partial Z} \\ \frac{\partial N_I}{\partial X}\frac{\partial x}{\partial Y} + \frac{\partial N_I}{\partial Y}\frac{\partial x}{\partial X} & \frac{\partial N_I}{\partial X}\frac{\partial y}{\partial Y} + \frac{\partial N_I}{\partial Y}\frac{\partial y}{\partial X} & \frac{\partial N_I}{\partial X}\frac{\partial z}{\partial Y} + \frac{\partial N_I}{\partial Y}\frac{\partial z}{\partial X} \\ \frac{\partial N_I}{\partial X}\frac{\partial x}{\partial Z} + \frac{\partial N_I}{\partial Z}\frac{\partial x}{\partial X} & \frac{\partial N_I}{\partial X}\frac{\partial y}{\partial Z} + \frac{\partial N_I}{\partial Z}\frac{\partial y}{\partial X} & \frac{\partial N_I}{\partial X}\frac{\partial z}{\partial Z} + \frac{\partial N_I}{\partial Z}\frac{\partial z}{\partial X} \\ \frac{\partial N_I}{\partial Y}\frac{\partial x}{\partial Z} + \frac{\partial N_I}{\partial Z}\frac{\partial x}{\partial Y} & \frac{\partial N_I}{\partial Y}\frac{\partial y}{\partial Z} + \frac{\partial N_I}{\partial Z}\frac{\partial y}{\partial Y} & \frac{\partial N_I}{\partial Y}\frac{\partial z}{\partial Z} + \frac{\partial N_I}{\partial Z}\frac{\partial z}{\partial Y} \end{bmatrix} \text{ in 3D} \tag{4.16}$$

Finally the $\boldsymbol{B}_0$ can be built as :

$$\boldsymbol{B}_0 = \begin{bmatrix} \boldsymbol{B}_1^0 & \boldsymbol{B}_2^0 & \boldsymbol{B}_3^0 & \cdots & \boldsymbol{B}_m^0 \end{bmatrix} \text{ where m is the number of nodes in that element.}$$

We are now able to define the internal nodal forces in Voigt Notation(Appendix B) as:

$$\boldsymbol{f}_I^{\text{int}} = \int_{\Omega_0} \frac{\partial N_I}{\partial X_j} F_{jk} S_{ik} d\Omega_0 = \int_{\Omega_0} \left(\boldsymbol{B}_I^0\right)^T \{\boldsymbol{S}\} d\Omega_0 \tag{4.17}$$

The Mass matrix is defined as:

$$M_{ijIJ} = \delta_{ij} \int_{\Omega_0} \rho_0 N_I N_J d\Omega_0 \tag{4.18}$$

And the discrete form of the principle of virtual work ends up yielding,

$$\underbrace{\int_{\Omega_0} N_I \rho_0 \ddot{u}_i d\Omega_0}_{M\boldsymbol{a}} + \underbrace{\int_{\Omega_0} \left(\boldsymbol{B}_I^0\right)^T \{\boldsymbol{S}\} d\Omega_0}_{\boldsymbol{f}_{\text{int}}} = \underbrace{\int_{\Omega_0} \rho_0 b_i d\Omega_0 + \int_{\Gamma^0{}_N} t^0{}_i d\Gamma}_{\boldsymbol{f}_{\text{ext}}} \tag{4.19}$$

Chapter 5

Linearized Equations and Solution methods

5.1 Introduction

Once NonLinear Finite Element Discretizations have been stated, it is time to describe the solution methods. For transient problems, it is needed to implement some kind of time integration scheme. In our case, implicit time integration has been chosen, particularly the Newmark β-method. To solve the discrete equations, the application of a nonlinear method will be needed, such as Newton-Raphson method. As it will be seen, Newton method may not converge in some special problems and line search methods must be invoked.

A critical step in the solution of the Nonlinear Solids problem is the linearization of the governing equations. Linearization procedures are described later in this chapter.

To be able to combine both the transient and the static problem, let us write the discrete momentum equation at time step $n+1$ as:

$$s_D \boldsymbol{M}\boldsymbol{a}^{n+1} + \boldsymbol{f}_{\text{int}}\left(\boldsymbol{d}^{n+1}, t^{n+1}\right) - \boldsymbol{f}_{\text{ext}}\left(\boldsymbol{d}^{n+1}, t^{n+1}\right) = \boldsymbol{r}\left(\boldsymbol{d}^{n+1}, t^{n+1}\right) = 0 \tag{5.1}$$

where s_D is a switch parameter such that

$$s_D = \begin{cases} 0 \text{ for a static (equilibrium) problem} \\ 1 \text{ for a dynamic (transient) problem} \end{cases}$$

The column matrix $\boldsymbol{r}\left(\boldsymbol{d}^{n+1}, t^{n+1}\right)$ is called a residual. Note that when the solution has been achieved, the residual vanishes. The discrete equations are nonlinear algebraic equations in the nodal displacements, $\boldsymbol{d}^{n+1}$.

5.2 Implicit Time Integration Scheme: The Newmark β-equations

The Newmark β-method is a well-known class of time integrators. For this time integrator, the updated displacements and velocities are given by

$$\boldsymbol{d}^{n+1} = \widetilde{\boldsymbol{d}}^{n+1} + \beta \Delta t^2 \boldsymbol{a}^{n+1} \qquad \text{where} \qquad \widetilde{\boldsymbol{d}}^{n+1} = \boldsymbol{d}^n + \Delta t \boldsymbol{v}^n + \frac{\Delta t^2}{2}(1-2\beta)\boldsymbol{a}^n \tag{5.2}$$

$$\boldsymbol{v}^{n+1} = \widetilde{\boldsymbol{v}}^{n+1} + \gamma \Delta t \boldsymbol{a}^{n+1} \qquad \text{where} \qquad \widetilde{\boldsymbol{v}}^{n+1} = \boldsymbol{v}^n + (1-\gamma)\Delta t \boldsymbol{a}^n \tag{5.3}$$

where Δt is the time interval between time at step $n+1$ and time at step n, $\Delta t = t^{n+1} - t^n$. The scheme is fully dependent on the parameters β and γ. The parameter γ controls artificial viscosity, a damping introduced by the numerical method. When $\gamma > \frac{1}{2}$ then artificial damping is added.

Regarding to the stability of the method, it is unconditionally stable for values β and γ such that:

$$\beta \geq \frac{\gamma}{2} \geq \frac{1}{4} \tag{5.4}$$

It is easy to see that γ must be greater than or equal to $\frac{1}{2}$ to ensure that the method is unconditionally stable. However, when $\gamma > \frac{1}{2}$ the method is adding artificial damping. Therefore, the best value for the parameter γ is $\frac{1}{2}$. With respect to β, it must be greater than or equal to $\frac{1}{4}$ for the optimal value of γ. Particularly, when $\beta = \frac{1}{4}$ the undamped trapezoidal rule is applied. Let us underline, that when $\beta = 0$ then we recover the explicit central difference method. For this thesis, we are going to consider only implicit schemes, so that $\beta > 0$.

By using equation 5.2 we can isolate the acceleration at time step $n+1$.

$$\boldsymbol{a}^{n+1} = \frac{1}{\beta \Delta t^2}\left(\boldsymbol{d}^{n+1} - \widetilde{\boldsymbol{d}}^{n+1}\right) \tag{5.5}$$

and substituting this expression into the discrete momentum equation 5.1, it gives

$$\frac{s_D}{\beta \Delta t^2}\boldsymbol{M}\left(\boldsymbol{d}^{n+1} - \widetilde{\boldsymbol{d}}^{n+1}\right) + \boldsymbol{f}_{\text{int}}\left(\boldsymbol{d}^{n+1}, t^{n+1}\right) - \boldsymbol{f}_{\text{ext}}\left(\boldsymbol{d}^{n+1}, t^{n+1}\right) = \boldsymbol{r}\left(\boldsymbol{d}^{n+1}, t^{n+1}\right) = 0 \tag{5.6}$$

so the discrete problem for both the transient and the static problem states per each time step: find $\boldsymbol{d}^{n+1}$ so that $\boldsymbol{r}\left(\boldsymbol{d}^{n+1}, t^{n+1}\right) = 0$.

5.3 Newton's method

When one wants to solve nonlinear system of algebraic equations the most widely used and most robust method is Newton's method. The solution of the system by Newton's method is an iterative procedure. The iteration number is indicated as i. So that $\boldsymbol{d}_i^{n+1}$ would be the solution at time step $n+1$ for the iteration number i. To begin the iterative procedure, a starting value for the unknown must be chosen; usually the solution $\boldsymbol{d}^n$ from the last time step is selected, so $\boldsymbol{d}_0^{n+1} \equiv \boldsymbol{d}^n$. In dynamic problems, when working with the Newmark β-method, a better starting value is $\widetilde{\boldsymbol{d}}^{n+1}$.

If we consider a Taylor expansion of the residual about the current value of the nodal displacement $\boldsymbol{d}_i^{n+1}$ and setting the resulting residual equal to zero:

$$\boldsymbol{r}\left(\boldsymbol{d}_i^{n+1}, t^{n+1}\right) + \frac{\partial \boldsymbol{r}\left(\boldsymbol{d}_i^{n+1}, t^{n+1}\right)}{\partial \boldsymbol{d}} \Delta \boldsymbol{d} + \mathscr{O}\left(\Delta \boldsymbol{d}^2\right) = \boldsymbol{0} \tag{5.7}$$

The matrix $\boldsymbol{A} = \frac{\partial \boldsymbol{r}\left(\boldsymbol{d}_i^{n+1}, t^{n+1}\right)}{\partial \boldsymbol{d}}$ is called *the system Jacobian matrix*. Dropping higher-order terms, Equation 5.7 gives

$$\boldsymbol{r} + \boldsymbol{A}\Delta \boldsymbol{d} = \boldsymbol{0} \tag{5.8}$$

The increment in the nodal displacements in the Newton iterative procedure is obtained by solving a system of linear algebraic equations

$$\boldsymbol{A}\Delta \boldsymbol{d} = -\boldsymbol{r}\left(\boldsymbol{d}_i^{n+1}, t^{n+1}\right) \tag{5.9}$$

Once the increments in nodal displacements have been obtained, they are added to the previous iterate

$$\boldsymbol{d}_{i+1}^{n+1} = \boldsymbol{d}_i^{n+1} + \Delta \boldsymbol{d} \tag{5.10}$$

The process is repeated until convergence is met. The Jacobian matrix must be computed. From equation 5.6 we can write the Jacobian for the Newmark integrator as

$$\boldsymbol{A} = \frac{\partial \boldsymbol{r}}{\partial \boldsymbol{d}} = \frac{\partial}{\partial \boldsymbol{d}}\left(\frac{s_D}{\beta \Delta t^2}\boldsymbol{M}\left(\boldsymbol{d}^{n+1} - \widetilde{\boldsymbol{d}}^{n+1}\right) + \boldsymbol{f}_{\text{int}} - \boldsymbol{f}_{\text{ext}}\right) = \frac{s_D}{\beta \Delta t^2}\boldsymbol{M} + \frac{\partial \boldsymbol{f}_{\text{int}}}{\partial \boldsymbol{d}} - \frac{\partial \boldsymbol{f}_{\text{ext}}}{\partial \boldsymbol{d}} \tag{5.11}$$

The Jacobian of the internal nodal forces is called *the tangent stiffness matrix* and will be denoted as $\boldsymbol{K}_{\text{int}}$. The Jacobian of the external nodal forces is called *the load stiffness matrix* and is denoted as $\boldsymbol{K}_{\text{ext}}$. Therefore, the final form of the Jacobian matrix yields

$$\boldsymbol{A} = \frac{s_D}{\beta \Delta t^2}\boldsymbol{M} + \boldsymbol{K}_{\text{int}} - \boldsymbol{K}_{\text{ext}} \tag{5.12}$$

To find out expressions for the tangent stiffness matrix $\boldsymbol{K}_{\text{int}}$ and the load stiffness matrix $\boldsymbol{K}_{\text{ext}}$ it will be needed to linearize both expressions. Both $\boldsymbol{K}_{\text{int}}$ and $\boldsymbol{K}_{\text{ext}}$ will be explained in the following section 5.4.

To end this section, let us introduce the flowchart for solving the nonlinear problem by considering the Newmark β-method as the time integrator scheme:

Algorithm 1: Flowchart for Newton-Raphson scheme with Newmark β-method

---

1. Introduce initial conditions for both the velocity $\boldsymbol{v}^0$, and displacement $\boldsymbol{d}^0$. Stresses $\boldsymbol{\sigma}^0$ must be computed according with the constitutive equation. Also, the parameters which control the time step $n = 0$ and the time itself $t = t_0$need to be initialized.

2. It is important to see that even though our initial parameters can be considered zero, the initial forces may not vanish for the initial state. Therefore, both the external and the internal ones must be computed according to the expressions (4.6) or (4.19) depending on the formulation considered,

$$\boldsymbol{f}^0 = \boldsymbol{f}\left(\boldsymbol{d}^0, t_0\right) = \boldsymbol{f}_{\text{ext}}\left(\boldsymbol{d}^0, t_0\right) - \boldsymbol{f}_{\text{int}}\left(\boldsymbol{d}^0, t_0\right)$$

3. Compute the initial accelerations of the system according to

$$\boldsymbol{a}^0 = \boldsymbol{M}^{-1}\boldsymbol{f}^0$$

   where the mass matrix $\boldsymbol{M}$ is computed according to (4.7) and (4.18) depending on the formulation considered.

4. It is time to estimate our solution. For the transient problem, $\boldsymbol{d}_0^{n+1} = \widetilde{\boldsymbol{d}}^{n+1}$ where $\widetilde{\boldsymbol{d}}^{n+1}$ is computed according to Equation (5.2). For the static problem we will consider $\boldsymbol{d}_0^{n+1} = \boldsymbol{d}^n$. We consider here any time step n and its corresponding time t_n. We compute the time step at $n+1$ as $t_{n+1} = t_n + \Delta t$

5. Here, we start the iterative Newton procedure for time step $n+1$, iteration i

   (a) We need to compute the forces for our estimate solution,

$$\boldsymbol{f}_i^{n+1} = \boldsymbol{f}\left(\boldsymbol{d}_i^{n+1}, t_{n+1}\right) = \boldsymbol{f}_{\text{ext}}\left(\boldsymbol{d}_i^{n+1}, t_{n+1}\right) - \boldsymbol{f}_{\text{int}}\left(\boldsymbol{d}_i^{n+1}, t_{n+1}\right)$$

(b) Thanks to the Newmark β-equations we can compute an estimation of both the velocity and the acceleration at time step $n+1$

$$\boldsymbol{a}_i^{n+1} = \frac{1}{\beta \Delta t^2}\left(\boldsymbol{d}_i^{n+1} - \widetilde{\boldsymbol{d}}^{n+1}\right), \qquad \boldsymbol{v}_i^{n+1} = \widetilde{\boldsymbol{v}}^{n+1} + \gamma \Delta t \boldsymbol{a}_i^{n+1}$$

Let us recall that both $\widetilde{\boldsymbol{d}}^{n+1}$ and $\widetilde{\boldsymbol{v}}^{n+1}$ only depends upon the estimation at the beginning of the time step so that they must not be updated each Newton iteration.

(c) We can compute now the residual for this iteration as:

$$\boldsymbol{r}_i^{n+1} = \boldsymbol{M}\boldsymbol{a}_i^{n+1} - \boldsymbol{f}_i^{n+1}$$

(d) Compute the Jacobian $\boldsymbol{A}\left(\boldsymbol{d}_i^{n+1}\right)$ will be also needed according with expression (5.12).

(e) It is time to consider essential boundary conditions and modify $\boldsymbol{A}\left(\boldsymbol{d}_i^{n+1}\right)$ when needed.

(f) We can solve the linear system of equations given by:

$$\Delta \boldsymbol{d} = -\boldsymbol{A}^{-1}\left(\boldsymbol{d}_i^{n+1}\right) \cdot \boldsymbol{r}_i^{n+1}$$

(g) Update the solution for the next iteration $\boldsymbol{d}_{i+1}^{n+1} = \boldsymbol{d}_i^{n+1} + \Delta \boldsymbol{d}$

(h) Check convergence criterion. In our case, we compute $\boldsymbol{r}_{i+1}^{n+1}$ and compare it with a tolerance value. If this value is not met, then we start another Newton iteration by repeating the procedure from step 5.

6. Once convergence criterion is met, we update the displacements for step $n+1$ as $\boldsymbol{d}^{n+1} = \boldsymbol{d}_{i+1}^{n+1}$, and we update the values of the time step $n+1 \to n$ and $t_{n+1} \to t_n$. We start the next time step by repeating the procedure from step 4.

5.4 Linearization

Let us separate the linearization of the internal nodal forces and the external ones.

5.4.1 Linearization of internal nodal forces

First of all let us recall the expression of the internal nodal forces in the Total Lagrangian form given by

$$\boldsymbol{f}_{\text{int}} = \int_{\Omega_0} \frac{\partial N_I}{\partial X_j} P_{ji} d\Omega_0 \tag{5.13}$$

Taking the material time derivative gives

$$\frac{\partial \boldsymbol{f}_{\text{int}}}{\partial t} = \dot{\boldsymbol{f}}_{\text{int}} = \int_{\Omega_0} \frac{\partial N_I}{\partial X_j} \dot{P}_{ji} d\Omega_0 \tag{5.14}$$

To obtain $\boldsymbol{K}_{\text{int}}$, stress rate $\dot{\boldsymbol{P}}$ will be expressed in terms of the nodal velocities through the constitutive equation and the strain measure. However, constitutive equations are expressed in terms of the Second Piola-Kirchhoff stress rate $\dot{\boldsymbol{S}}$ when working in Total Lagrangian formulation, so it is worth to change the rate in function of $\boldsymbol{P}$ by the rate of $\boldsymbol{S}$. The material time derivative of $\boldsymbol{S}$ can be related to the one of the nominal stress $\boldsymbol{P}$ through the transformation $\boldsymbol{P} = \boldsymbol{S} \cdot \boldsymbol{F}^T$

$$\dot{\boldsymbol{P}} = \dot{\boldsymbol{S}} \cdot \boldsymbol{F}^T + \boldsymbol{S} \cdot \dot{\boldsymbol{F}}^T \tag{5.15}$$

Substituting this expression in Equation 5.14 it gives

$$\dot{\boldsymbol{f}}_{\text{int}} = \frac{\partial \boldsymbol{f}_{\text{int}}}{\partial t} = \frac{\partial \boldsymbol{f}_{\text{int}}}{\partial \boldsymbol{d}} \frac{\partial \boldsymbol{d}}{\partial t} = \boldsymbol{K}_{\text{int}} \dot{\boldsymbol{d}} = \int_{\Omega_0} \frac{\partial N_I}{\partial X_j} \dot{P}_{ji} d\Omega_0 = \int_{\Omega_0} \frac{\partial N_I}{\partial X_j} \left(\dot{S}_{jr} F_{ir} + S_{jr} \dot{F}_{ir} \right) d\Omega_0 := \dot{\boldsymbol{f}}_{\text{mat}} + \dot{\boldsymbol{f}}_{\text{geo}} \tag{5.16}$$

The above equation shows that the rate of the internal nodal forces consists of two parts:

1. On the one hand, a first part which involves the rate of the Second Piola stress tensor and thus depends on the material response, $\dot{\boldsymbol{f}}_{\text{mat}}$. Note that here the current deformation gradient is being considered, so the geometric changes are not present in this expression. Only the current deformation state plays a role in it.

2. On the other hand, a part which involves the current state of stress and accounts for geometric effects of the deformation, $\dot{\boldsymbol{f}}_{\text{geo}}$.

The idea is to develop expressions for both the geometric and the material rate of the internal forces .

5.4.1.1 Material Tangent Stiffness

According with the expression of the rate of internal force, and the definition of the material rate of them,

$$\dot{\boldsymbol{f}}_{\text{mat}} = \int_{\Omega_0} \frac{\partial N_I}{\partial X_j} \dot{S}_{jr} F_{ir} d\Omega_0 = \int_{\Omega_0} \boldsymbol{B}_0^T \left\{\dot{\boldsymbol{S}}\right\} d\Omega_0 \tag{5.17}$$

where the definition of $\boldsymbol{B}_0^T$ (Equation **??**) has been applied and Voigt Notation (Appendix B) is considered. Taking into account the constitutive equation in rate form

$$\dot{S}_{ij} = \mathbb{C}_{ijkl} \dot{E}_{kl} \qquad \text{or} \qquad \left\{\dot{\boldsymbol{S}}\right\} = \{\mathbb{C}\} \left\{\dot{\boldsymbol{E}}\right\} \tag{5.18}$$

It can be easily shown that $\boldsymbol{B}_0$ relates the rate of Green strain $\dot{\boldsymbol{E}}$ to the node velocities by

$$\left\{\dot{\boldsymbol{E}}\right\} = \boldsymbol{B}_0 \dot{\boldsymbol{d}} \tag{5.19}$$

Therefore,

$$\left\{\dot{\boldsymbol{S}}\right\} = \{\mathbb{C}\} \left\{\dot{\boldsymbol{E}}\right\} = \{\mathbb{C}\} \boldsymbol{B}_0 \dot{\boldsymbol{d}} \tag{5.20}$$

and including this expression into Equation 5.17 it gives

$$\dot{\boldsymbol{f}}_{\text{mat}} = \int_{\Omega_0} \boldsymbol{B}_0^T \left\{\dot{\boldsymbol{S}}\right\} d\Omega_0 = \int_{\Omega_0} \boldsymbol{B}_0^T \{\mathbb{C}\} \boldsymbol{B}_0 \dot{\boldsymbol{d}} d\Omega_0 = \left(\underbrace{\int_{\Omega_0} \boldsymbol{B}_0^T \{\mathbb{C}\} \boldsymbol{B}_0 d\Omega_0}_{\boldsymbol{K}_{\text{mat}}} \right) \dot{\boldsymbol{d}} := \boldsymbol{K}_{\text{mat}} \dot{\boldsymbol{d}} \tag{5.21}$$

So the Material Tangent Stiffness $\boldsymbol{K}_{\text{mat}}$, is the tensor which allows us to relate the material rate of internal nodal forces with the rate of nodal displacements.

To convert this expression to Updated Lagrangian formulation we have to transform the current configuration to be the reference one. By doing this, it is obtained that $\boldsymbol{B}_0 \to \boldsymbol{B}$, $\boldsymbol{S} \to \boldsymbol{\sigma}$ and the domain $\Omega \to \Omega_0$. So the expression of $\boldsymbol{K}_{\text{mat}}$ in Updated formulation emerges as

$$\boldsymbol{K}_{\text{mat}} = \int_{\Omega} \boldsymbol{B}^T \{\mathbb{C}\} \boldsymbol{B} d\Omega_0 \tag{5.22}$$

where now $\mathbb{C}$ is the constitutive tensor which relates the Cauchy stress $\boldsymbol{\sigma}$ and the Almansi strain tensor $\boldsymbol{e}$. The expression of $\boldsymbol{B}$ can be found in Equation 4.9.

5.4.1.2 Geometric Stiffness

First of all, let us recover the expression of the geometric rate of the internal nodal forces,

$$\dot{\boldsymbol{f}}_{\text{geo}} = \int_{\Omega_0} \frac{\partial N_I}{\partial X_j} S_{jr} \dot{F}_{ir} d\Omega_0 \tag{5.23}$$

Let us study the rate of the deformation gradient $\boldsymbol{F}$:

$$\dot{F}_{ir} = \frac{\partial}{\partial t}(F_{ir}) = \frac{\partial}{\partial t}\left(\frac{\partial x_i(\boldsymbol{X},t)}{\partial X_r}\right) = \frac{\partial}{\partial t}\left(\frac{\partial N_I(\boldsymbol{X}) x_{Ii}(t)}{\partial X_r}\right) = \frac{\partial N_I(\boldsymbol{X})}{\partial X_r} \cdot \frac{\partial}{\partial t} x_{Ii}(t) := \beta^0_{Ir} \dot{d}_{iJ} \tag{5.24}$$

where the approximation of the nodal coordinates has been applied. A new matrix has been defined, $\boldsymbol{\beta}^0$ which includes the directional derivatives of the shape functions with respect to the material coordinates:

$$\boldsymbol{\beta}^0_I = \begin{bmatrix} \frac{\partial N_I}{\partial X} \\ \frac{\partial N_I}{\partial Y} \end{bmatrix} \text{ in 2D and } \boldsymbol{\beta}^0_I = \begin{bmatrix} \frac{\partial N_I}{\partial X} \\ \frac{\partial N_I}{\partial Y} \\ \frac{\partial N_I}{\partial Z} \end{bmatrix} \text{ in 3D} \tag{5.25}$$

The $\boldsymbol{\beta}^0$ matrix is built by adding each one of the submatrices $\boldsymbol{\beta}^0_I$ per each node of the element such that

$$\boldsymbol{\beta}_0 = \begin{bmatrix} \boldsymbol{\beta}^0_1 & \boldsymbol{\beta}^0_2 & \boldsymbol{\beta}^0_3 & \cdots & \boldsymbol{\beta}^0_m \end{bmatrix} \text{ where m is the number of nodes in that element.}$$

Coming back to the definition of the geometric rate of the internal nodal forces, it is obtained

$$\dot{\boldsymbol{f}}_{\text{geo}} = \int_{\Omega_0} \frac{\partial N_I}{\partial X_j} S_{jr} \dot{F}_{ir} d\Omega_0 = \int_{\Omega_0} \beta^0_{Ij} S_{jr} \beta^0_{rJ} \dot{d}_{iJ} \delta_{ik} d\Omega_0 = \left(\underbrace{\int_{\Omega_0} \beta^0_{Ij} S_{jr} \beta^0_{rJ} d\Omega_0 \delta_{ik}}_{\boldsymbol{K}_{\text{geo}}} \right) \dot{d}_{iJ} := \boldsymbol{K}_{\text{geo}} \dot{\boldsymbol{d}} \tag{5.26}$$

where the delta Kronecker δ_{ik} must have been applied to match indexes. Finally, the Geometric Stiffness $\boldsymbol{K}_{\text{geo}}$ emerges as the tensor which allows us to relate the geometric rate of internal forces with the rate of nodal displacements. The inditial expression of $\boldsymbol{K}_{\text{geo}}$ is

$$\boldsymbol{K}_{\text{geo}} = \boldsymbol{I} \int_{\Omega_0} \left(\boldsymbol{\beta}^0\right)^T \boldsymbol{S} \boldsymbol{\beta}^0 d\Omega_0 \tag{5.27}$$

To obtain the expression of $\boldsymbol{K}_{\text{geo}}$ for the Updated Lagrangian formulation it is only needed to convert again the current configuration into the reference one. In this case, $\boldsymbol{\beta}_0 \rightarrow \boldsymbol{\beta}$, the stresses $\boldsymbol{S} \rightarrow \boldsymbol{\sigma}$ and the domain Ω_0 becomes Ω. The just defined $\boldsymbol{\beta}$ matrix is defined exactly in the same way as $\boldsymbol{\beta}^0$ but it accounts the derivatives with respect to the spatial coordinates rather than the material ones. The Geometric Stiffness for the Updated formulation yields,

$$\boldsymbol{K}_{\text{geo}} = \boldsymbol{I} \int_{\Omega} (\boldsymbol{\beta})^T \boldsymbol{\sigma} \boldsymbol{\beta} d\Omega \tag{5.28}$$

At the end of this procedure, the expressions to compute the tangent stiffness matrix $\boldsymbol{K}_{\text{int}}$ have been obtained,

$$\frac{\partial \boldsymbol{f}_{\text{int}}}{\partial \boldsymbol{d}} = \boldsymbol{K}_{\text{int}} = \boldsymbol{K}_{\text{mat}} + \boldsymbol{K}_{\text{geo}}$$

5.4.2 External load stiffness

In several geometrically nonlinear problems there are some external loads which vary with changes of the body configuration. They are called follower loads. These loads vary during the movement of the solid and changes the external nodal forces. The external load stiffness $\boldsymbol{K}_{\text{ext}}$ takes into account these effects in the Jacobian matrix.

$\boldsymbol{K}_{\text{ext}}$ is the tensor which relates the rate of the external nodal forces to the rate of nodal displacements. In this work these forces are not going to be considered $\boldsymbol{K}_{\text{ext}} = \boldsymbol{0}$ but it is worth to name them to know about their function.

5.5 Line Search method

Let us recover the iterative procedure scheme with Newton-Raphson method,

$$\boldsymbol{A}\Delta\boldsymbol{d} = -\boldsymbol{r}\left(\boldsymbol{d}_i^{n+1}, t^{n+1}\right) \longrightarrow \boldsymbol{d}_{i+1}^{n+1} = \boldsymbol{d}_i^{n+1} + \Delta\boldsymbol{d} \tag{5.29}$$

It means that Newton method finds out a direction $\Delta\boldsymbol{d}$ and it applies a factor 1 to this direction. Line search methods try to find the optimal value ξ by minimizing a measure of the residual along the direction found by Newton scheme $\Delta\boldsymbol{d}$:

$$\boldsymbol{d}_{i+1}^{n+1} = \boldsymbol{d}_i^{n+1} + \xi \cdot \Delta\boldsymbol{d} \tag{5.30}$$

When the process of finding this optimal value ξ is cheaper than computing a new direction by using a new Jacobian, this methods are quite useful and the effectiveness of Newton method

is increased. Line search methods are considered as a powerful tool to insert in the iterative Newton scheme to work together.

At the minimum, the residual $\boldsymbol{r}$ must be orthogonal to the direction of advance $\boldsymbol{\Delta d}$. This condition can be expressed as a scalar equation for ξ:

$$R(\xi) = \Delta \boldsymbol{d}^T \cdot \boldsymbol{r}\left(\boldsymbol{d}_i^{n+1} + \xi \cdot \Delta \boldsymbol{d}\right) = 0 \tag{5.31}$$

In addition, when the system is conservative, if we consider that at the end of the iteration the total potential energy W is minimized in the direction of $\Delta \boldsymbol{d}$ then,

$$\frac{\partial W}{\partial \xi} = \frac{\partial W}{\partial \boldsymbol{d}} \frac{\partial \boldsymbol{d}}{\partial \xi} = \boldsymbol{r}^T \Delta \boldsymbol{d} = 0 \tag{5.32}$$

Thus, finding the minimum of the potential energy with respect to the ξ-parameter is equivalent to find the value ξ that verifies equation 5.31. One of the long term goals of this work is end up studying Fluid-Structure Interaction. In this kind of problems, transient problem is considered in the solid domain and the problem is not conservative anymore. So we are interested in using a Line search method which can be applied in non-conservative systems.

First of all, Working only with descent directions is wanted , in our case it means that,

$$R(0) = \Delta \boldsymbol{d}^T \cdot \boldsymbol{r}\left(\boldsymbol{d}_i^{n+1} + 0 \cdot \Delta \boldsymbol{d}\right) < 0$$

Thus, if the scalar function $R(0) > 0$ for a given direction $\Delta \boldsymbol{d}$, we are going to flip the direction $\Delta \boldsymbol{d} = -\Delta \boldsymbol{d}$ to enforce our direction to be a descent one.

Due to the extreme nonlinearity of the scalar function $R(\xi)$, finding a solution of problem 5.31 is very expensive and it is sufficient to obtain a value of ξ such that,

$$| R(\xi) | < \rho \, | R(0) | \tag{5.33}$$

where a typical value of $\rho = 0.5$ is selected.

When the value of standard Newton-Raphson ($\xi = 1$) does not satisfy this condition, we can apply the following method:

It is convenient to approximate $R(\xi)$ as a quadratic function in ξ . We know the value of the function when $\xi = 0$,

$$R(0) = \Delta \boldsymbol{d}^T \cdot \boldsymbol{r}\left(\boldsymbol{d}_i^{n+1} + 0 \cdot \Delta \boldsymbol{d}\right) = \Delta \boldsymbol{d}^T \cdot \boldsymbol{r}\left(\boldsymbol{d}_i^{n+1}\right) \tag{5.34}$$

which is computed with the value already calculated of the residual in the already converged state. Moreover, we can easily relate the value of the derivative of this function with respect

to ξ when $\xi = 0$,

$$\frac{dR}{d\xi}(0) = \frac{d}{d\xi}\left\{\Delta \boldsymbol{d}^T \cdot \boldsymbol{r}\left(\boldsymbol{d}_i^{n+1}\right)\right\} = \Delta \boldsymbol{d}^T \underbrace{\frac{\partial \boldsymbol{r}\left(\boldsymbol{d}_i^{n+1}\right)}{\partial \boldsymbol{d}}}_{\boldsymbol{A}\left(\boldsymbol{d}_i^{n+1}\right)} \Delta \boldsymbol{d} =$$

$$= \Delta \boldsymbol{d}^T \underbrace{\boldsymbol{A}\left(\boldsymbol{d}_i^{n+1}\right)\Delta \boldsymbol{d}}_{-\boldsymbol{r}\left(\boldsymbol{d}_i^{n+1}\right)} = -\Delta \boldsymbol{d}^T \boldsymbol{r}\left(\boldsymbol{d}_i^{n+1}\right) = -R(0) \tag{5.35}$$

As we want to implement a quadratic function, A third information about the function $R(\xi)$ is needed, typically the value of the function when $\xi = 1$ is computed,

$$R(1) = \Delta \boldsymbol{d}^T \cdot \boldsymbol{r}\left(\boldsymbol{d}_i^{n+1} + 1 \cdot \Delta \boldsymbol{d}\right) = \Delta \boldsymbol{d}^T \cdot \boldsymbol{r}\left(\boldsymbol{d}_i^{n+1} + \Delta \boldsymbol{d}\right) \tag{5.36}$$

The quadratic approximation is obtained as:

$$R(\xi) \approx (1-\xi)R(0) + R(1)\xi^2 \tag{5.37}$$

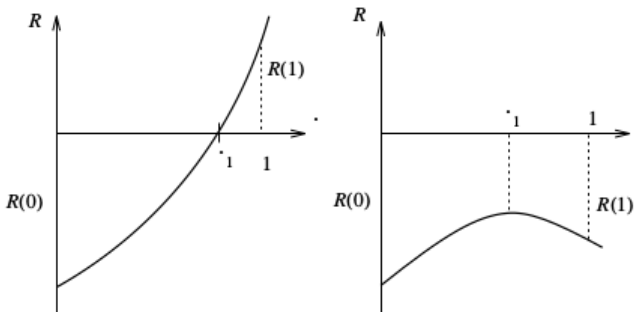

Figure 5.1: Quadratic Interpolation Line Search. From [6]

From the value $\alpha = \frac{R(0)}{R(1)}$ we are able to split the solution in two situations:

- When $\alpha < 0$ (Left plot in Figure 5.1) the square root is real and the solution emerges

$$\xi' = \frac{\alpha}{2} + \sqrt{\left(\frac{\alpha}{2}\right) - \alpha} \tag{5.38}$$

- Alternatively, when $\alpha > 0$ (Right plot in Figure 5.1) there is no solution. However, ξ'

can be easily obtained as the value that minimizes the quadratic function, which is

$$\xi' = \frac{\alpha}{2} \tag{5.39}$$

This procedure is repeated by substituting the value $\xi = 1$ by the new value ξ' and using $R(0), \frac{dR}{d\xi}(0)$ and $R(\xi')$ to obtain the next quadratic approximation of $R(\xi)$ until equation 5.33 is satisfied.

Chapter 6

Topological Derivative-based Topology Optimization of Nonlinear Structures

6.1 Introduction

The structural design problem can be addressed from different problems such as *Sizing optimization*, *Shape optimization* or *Topology optimization*. When the goal of our problem is to find the thickness of a known domain that minimizes (or maximizes) a physical quantity we are dealing with Sizing optimization. Alternatively, shape optimization tries to look for the optimum shape of one domain. On the other hand, Topology optimization involves the optimization of material layout within a given space. The design can attain any shape within the design space, instead of dealing with predefined configurations as the previous ones.

When developing topological optimization of continuous structures, there exist two approaches: the material and the geometrical approaches. The most known method of material approach is the *SIMP* methods (Solid Isotropic Microstructure with Penalization) [24]. In this method, a density field is considered $\rho(\boldsymbol{X}) \in [0,1]$ as the design variable so that in those areas where no material would be needed, we would find small values of ρ. One of the most used techniques for geometrical approach, we shall mention the *ESO* methods (Evolutionary Structural Optimization) [26] and the *TSA* methods (Topology Sensitivity Analysis) [1]. The line of action of both methods is to consider a cost function and measure the sensitivity, meaning, the variation of the cost function when some variation is induced in the geometry. The former methods make an approximation of the sensitivity based on finite differences when an element is removed in the mesh. The latter ones calculate the sensitivity when a small hole is created in the domain of the problem. The sensitivity of the cost function is described through a function which can be evaluated at any point of the geometry and is called *the topological*

derivative.

To develop a Topology optimization, there are several approaches which derive from different basis such as density approaches, level-set methods, phase-field methods, evolutionary methods, topological derivative among others and some of them can work together. In this work, we are interested in Topological Derivative-based Topology optimization which measures the sensitivity of a given shape functional with respect to an infinitesimal singular domain perturbation, such as the insertion of holes, inclusions or source-terms, mixed with a level-set method.

6.2 Topological Derivative

First of all let us comment that the expression of the topological derivative will be obtained in Total Lagrangian Formulation. For the sake of simplicity, let us neglect subscript 0 in this chapter.

As mentioned before, the topological derivative measures the sensitivity of creating a small hole for any point of the domain. Let $\Omega \subset \mathbb{R}^d$ with $(d = 2 \text{ or } d = 3)$ be an open bounded domain. The boundary of Ω, Γ is considered smooth enough to define almost everywhere $\boldsymbol{n}$ the unit normal vector. Let us now define the perturbed domain, $\Omega_\varepsilon \subset \mathbb{R}^d$, defined as the resulting domain of the extraction of a hole in the unperturbed domain Ω, $\Omega_\varepsilon = \Omega - \overline{B}_\varepsilon$. $\overline{B}_\varepsilon = B_\varepsilon \cup \partial B_\varepsilon$ is the ball of radius ε centered on the point $\tilde{\boldsymbol{X}}$(Figure 6.1) . Considering a cost function ψ, the topological derivative is written as [14]:

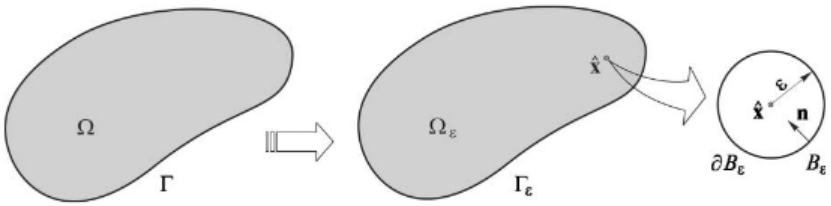

Figure 6.1: Original Topological Derivative concept. From [1]

$$D_T(\tilde{\boldsymbol{X}}) := \lim_{\varepsilon \to 0} \frac{\psi(\Omega_\varepsilon) - \psi(\Omega)}{f(\varepsilon)} \tag{6.1}$$

where $f(\varepsilon)$ is a function that decreases monotonically so that $f(\varepsilon) \to 0$ with $\varepsilon \to 0$. Let us remark that when the hole is created. there is no way to establish an homeomorphism between the perturbed and unperturbed domain. Therefore, the derivative cannot be obtained in a conventional way.

It is then proposed in [1] to start the problem with a hole $\overline{B}_\varepsilon$ already created and study the sensitivity of perturbing this hole with a small perturbation $\delta\varepsilon$ so that the hole $\overline{B}_\varepsilon$ becomes a different one $\overline{B}_{\varepsilon+\delta\varepsilon}$. Clearly, this perturbation allows us to define the remaining domain as $\Omega_{\varepsilon+\delta\varepsilon} = \Omega - \overline{B}_{\varepsilon+\delta\varepsilon}$ (Figure 6.2).

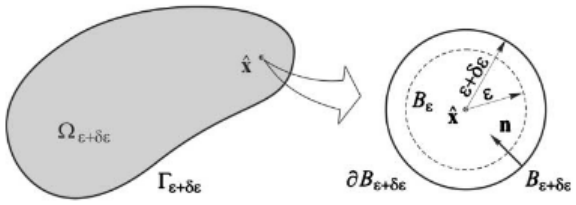

Figure 6.2: Modified Topological Derivative concept. From [1]

Moreover, it is also demonstrated in [7] that the topological derivative can be redefined as:

$$D_T(\tilde{\boldsymbol{X}}) := \lim_{\varepsilon\to 0}\left\{\lim_{\delta\varepsilon\to 0}\frac{\psi(\Omega_{\varepsilon+\delta\varepsilon})-\psi(\Omega_\varepsilon)}{f(\varepsilon+\delta\varepsilon)-f(\varepsilon)}\right\} \tag{6.2}$$

The advantage of the novel definition for the topological derivative is that the whole mathematical framework developed for the shape sensitivity analysis can be used, from now on, to compute the topological derivative. This action of increasing the hole can be interpreted as a sequence of configurations denoted by a parameter τ. This allows us to redefine the perturbation as a smooth and invertible mapping $\Upsilon(\boldsymbol{X},\tau)$ such that $\Upsilon(\boldsymbol{X},\tau=0)$ gives exactly the coordinates of the initial hole. In this way, we can define both domains Ω_ε and $\Omega_{\varepsilon+\delta\varepsilon}$ in terms of τ as $\Omega_{\varepsilon+\delta\varepsilon}\to\Omega_\tau$ and $\Omega_\varepsilon\to\Omega_{\tau=0}$. Moreover, for small values of τ the mapping $\boldsymbol{X}_\tau = \Upsilon(\boldsymbol{X},\tau)$ is written as

$$\boldsymbol{X}_\tau = \boldsymbol{X} + \tau\boldsymbol{V}(\boldsymbol{X}) \tag{6.3}$$

where $\boldsymbol{X}$ are the material coordinates of the initial hole. The shape design change is defined by $\boldsymbol{V}(\boldsymbol{X}) = \frac{\partial\Upsilon(\boldsymbol{X},\tau)}{\partial\tau}$. In fact, it can be proved that only the normal direction to the boundary Γ_ε gives meaningful results, V_n, [7]

$$\boldsymbol{X}_\tau = \boldsymbol{X} + \tau V_n\boldsymbol{n} \tag{6.4}$$

Taking into account that the perturbation $\delta\varepsilon$ is given by $\| \boldsymbol{X}_\tau - \boldsymbol{X} \|$ we can relate it with the parameter τ,

$$\delta\varepsilon = \| \boldsymbol{X}_\tau - \boldsymbol{X} \| = \| \tau V_n\boldsymbol{n} \| = \tau \mid V_n \mid \tag{6.5}$$

The definitions of the original topological derivative (Equation 6.1) and the modified one

(Equation 6.2) are normalized as

$$D_T(\tilde{\boldsymbol{X}}) = \frac{1}{|\,V_n\,|} \lim_{\varepsilon \to 0} \frac{1}{f'(\varepsilon)} \frac{d\psi(\Omega_\tau)}{d\tau} \tag{6.6}$$

The analytic form of the topological derivative for Nonlinear Solid Mechanics is still missing in the literature. In fact it is not possible to obtain an analytic solution for the problem as mentioned in [1]. However, [7] ,according with some papers, proposes to find a numerical expression for the topological derivative by running several interesting tests. In the paper, they manage to achieve the expression of the topological derivative as:

$$D_T(\tilde{\boldsymbol{X}}) = -\lim_{\varepsilon \to 0} \frac{1}{f'(\varepsilon)} \int_{\partial B_\varepsilon} \left(\frac{1}{2} \boldsymbol{S} : \boldsymbol{E} - \boldsymbol{b} \cdot \boldsymbol{u} \right) d\partial B_\varepsilon \tag{6.7}$$

With the absence of body forces $\boldsymbol{b} = \boldsymbol{0}$, they realized that:

$$D_T(\tilde{\boldsymbol{X}}) = \lim_{\varepsilon \to 0} d_T(\tilde{\boldsymbol{X}}) \quad \text{where} \quad d_T(\tilde{\boldsymbol{X}}) = -\frac{1}{f'(\varepsilon)} \int_{\partial B_\varepsilon} \left(\frac{1}{2} \boldsymbol{S} : \boldsymbol{E} \right) d\partial B_\varepsilon \tag{6.8}$$

This equation represents the analytic expression of the topological derivative except for the limit when $\varepsilon \to 0$. As mentioned before, this limit becomes impossible to solve analytically. However, an alternative procedure based on numerical experiments for the calculation of the limit is adopted. They consider a rectangular mesh with a hole placed in the center of it, and they compute numerically the value of $d_T(\tilde{\boldsymbol{X}})$ while decreasing the radius of the hole. It is observed that this integrand behaves as a constant in relation to the radius of the hole, so finally the topological derivative can be approximated up to a constant as

$$D_T(\tilde{\boldsymbol{X}}) \approx K \cdot \boldsymbol{S} : \boldsymbol{E} \tag{6.9}$$

Therefore, it is obtained an easy way to compute the topological derivative in any point of the mesh. The value of the constant K does not matter because we are only interested in seeing where the topological derivative becomes higher or smaller. Even though expression 6.9 does not give us the analytic expression for the topological derivative, it gives a numerical approach which fits perfectly in our purposes.

6.3 Topology Optimization applied to Nonlinear Solid Mechanics

Let Ω be the design or reference domain, $\Omega \subset \mathbb{R}^d$ with $(d = 2 \text{ or } d = 3)$ a bounded Lipschitz domain. The reference domain Ω is chosen so as to allow for a definition of the applied loads and boundary conditions. The boundary of Ω is decomposed into two disjoint parts $\partial\Omega := \Gamma = \Gamma_N \cup \Gamma_D$. The static non-linear elastic problem emerges as

$$\begin{cases} -\nabla.\boldsymbol{\sigma}(\boldsymbol{d}(\boldsymbol{X},t)) = \rho\left[\boldsymbol{b}(\boldsymbol{X},t) - \boldsymbol{a}(\boldsymbol{X},t)\right] & \text{in } \Omega \\ \boldsymbol{d}(\boldsymbol{X},t) = \overline{\boldsymbol{d}} & \text{on}\Gamma_D \\ \boldsymbol{\sigma}(\boldsymbol{d}(\boldsymbol{X},t))\cdot\boldsymbol{n} = \boldsymbol{t}(\boldsymbol{X},t) & \text{on } \Gamma_N \end{cases} \tag{6.10}$$

where $\boldsymbol{d}$ is the displacement field and unknown of the problem which depends on the material coordinates $\boldsymbol{X}$ and may depend upon time. $\boldsymbol{\sigma}$ is the Cauchy Stress tensor, $\boldsymbol{b}$ the body forces and $\boldsymbol{t}$ the surface ones, and $\boldsymbol{n}$ the unit outward normal vector to Γ.

Let us deal the problem with Total Lagrangian formulation, for that purpose , let us define the problem for the Second Piola-Kirchhoff stress tensor $\boldsymbol{S}$ and use the Green strain $\boldsymbol{E}$ as a measure of strains:

$$\begin{cases} -\nabla.\left[\frac{1}{J}\boldsymbol{F}\boldsymbol{S}\boldsymbol{F}^T\right] = \rho\left[\boldsymbol{b}(\boldsymbol{X},t) - \boldsymbol{a}(\boldsymbol{X},t)\right] & \text{in } \Omega \\ \boldsymbol{d}(\boldsymbol{X},t) = \overline{\boldsymbol{d}} & \text{on}\Gamma_D \\ \frac{1}{J}\boldsymbol{F}\boldsymbol{S}\boldsymbol{F}^T\cdot\boldsymbol{n} = \boldsymbol{t}(\boldsymbol{X},t) & \text{on } \Gamma_N \end{cases} \tag{6.11}$$

where transformation 2.17 has been considered. Thanks to the constitutive relation between the rate of stresses and the rate of strains we can relate them :

$$\dot{\boldsymbol{S}} = \mathbb{C} : \dot{\boldsymbol{E}} \tag{6.12}$$

where $\mathbb{C}$ is the fourth order constitutive tensor already explained.

In the topology optimization problem, the reference domain is split into two different subdomains Ω^+ and Ω^- such that $\Omega^+ \cap \Omega^- = \emptyset$ and $\Omega^+ \cup \Omega^- = \Omega$. Ω^+ represents a stiff material whereas Ω^- symbolizes a soft material. This subdivision into subdomains is easily represented trough a characteristic function χ such that:

$$\chi(\boldsymbol{X},t) = \begin{cases} 1 & \boldsymbol{X} \in \Omega^+ \\ 0 & \boldsymbol{X} \in \Omega^- \end{cases} \tag{6.13}$$

This function allows us to rewrite the constitutive tensor $\mathbb{C}$ in all the reference domain as

$$\mathbb{C} = \chi \mathbb{C}^{+} + (1-\chi)\mathbb{C}^{-} \tag{6.14}$$

where $\mathbb{C}^{+}$ and $\mathbb{C}^{-}$ are the constitutive tensors of the stiff and the soft material respectively. When simulating the soft material as void (absence of material in the areas where soft material should be placed) is wanted, the constitutive tensor $\mathbb{C}^{-}$ is considered as:

$$\mathbb{C}^{-} = \delta \cdot \mathbb{C}^{+} \tag{6.15}$$

where δ is a scalar parameter small enough to ensure that the soft material has almost no influence in the structure.

According with previous chapters, the discretization of the above problem yields for each time step n:

$$\frac{s_D}{\beta \Delta t^2} \boldsymbol{M} \left(\boldsymbol{d}^{n+1} - \tilde{\boldsymbol{d}}^{n+1} \right) + \boldsymbol{f}_{\text{int}} \left(\boldsymbol{d}^{n+1}, t^{n+1}, \chi \right) - \boldsymbol{f}_{\text{ext}} \left(\boldsymbol{d}^{n+1}, t^{n+1}, \chi \right) = \boldsymbol{r} \left(\boldsymbol{d}^{n+1}, t^{n+1}, \chi \right) = 0 \tag{6.16}$$

where equation 6.16 depends upon the characteristic parameter χ due to the effect of this parameter in the constitutive tensor $\mathbb{C}$ (Equation 6.14). The Topological Optimization problem tries to find the optimal domain such that it minimizes the structural compliance defined by the external forces $W_{\boldsymbol{f}_{\text{ext}}}(\chi)$. Thus, the Topological Optimization problem is formulated as follows:

$$\begin{aligned} &\min_{\chi \in \Omega_L} J(\chi) = W_{\boldsymbol{f}_{\text{ext}}}(\chi) \\ &\text{such that } \boldsymbol{r} \left(\boldsymbol{d}^{n+1}, t^{n+1}, \chi \right) = 0, \end{aligned} \tag{6.17}$$

where Ω_L is the feasible domain restricted to a volume constraint denoted as a fraction $0 < L < 1$ of the whole reference domain Ω, whose volume is denoted as $|\,\Omega\,|$,

$$\Omega_L = \left\{ \chi, \int_{\Omega} \chi d\Omega = L \,|\, \Omega \,| \right\} \tag{6.18}$$

In order to solve problem 6.17 as commented previously, we use the topological derivative concept together with a level-set method to advance iteratively to the optimal solution. To do that, a new function must be defined, which will be called the signed topological derivative,

such that:

$$\overline{D_T}(\boldsymbol{X},\chi) = \begin{cases} +\boldsymbol{S}:\boldsymbol{E} & \text{in } \boldsymbol{X} \in \Omega^+ \\ -\boldsymbol{S}:\boldsymbol{E} & \text{in } \boldsymbol{X} \in \Omega^- \end{cases} \tag{6.19}$$

To understand the sense of this function, we have to analyze the problem. Once the optimal value of the characteristic function is reached, it means, the value which satisfies equation 6.17, as the value of the topological derivative is always greater or equal than zero, the signed topological derivative must satisfy,

$$\overline{D_T}(\boldsymbol{X},\chi) \geq \overline{D_T}(\boldsymbol{Y},\chi)\ \forall \boldsymbol{X} \in \Omega^+,\ \forall \boldsymbol{Y} \in \Omega^- \tag{6.20}$$

This property of the signed topological derivative leads us naturally to construct a level set function $\omega(\boldsymbol{X},\chi)$ which will be able to differentiate between Ω^+ and Ω^-. In order to ensure that the volume restriction in the optimal topology is fulfilled, a scalar $\alpha \in \mathbb{R}$ must be introduced in the definition of ω,

$$\omega(\boldsymbol{X},\chi) = \overline{D_T}(\boldsymbol{X},\chi) + \alpha \tag{6.21}$$

Thus, the value α must be computed in such a way that it allows us to fulfill the volume constraint. To do that, we can use the Heaviside step function to impose that:

$$\int_\Omega H(\omega(\boldsymbol{X},\chi))\, d\Omega = L \mid \Omega \mid \tag{6.22}$$

where $H(\omega)$ is the Heaviside function, defined as

$$H(\omega) = \begin{cases} 1 & \text{if } \omega \geq 0 \\ 0 & \text{if } \omega < 0 \end{cases} \tag{6.23}$$

It is easy to see with equation 6.13 that, for the value χ which satisfies equation 6.17,

$$\chi = H(\omega) \tag{6.24}$$

6.4 Iterative Topology Optimization Algorithm

According with Section 6.3, we are able to introduce an iterative approach to solve the Topology Optimization problem applied to Nonlinear Solid Mechanics (Equation 6.17). To start the iterative procedure, an initial value for the level-set function ω^0 is needed to be set . Let us

take a unit initial value for the whole domain, considering that the whole domain is composed only by stiff material.

$$\omega^0\left(\boldsymbol{X},\chi^0\right)=\omega^0=1 \qquad \text{in } \Omega \tag{6.25}$$

where the subscript indicates iteration number. As we state in equation 6.24, for the characteristic function which satisfies the Topology Optimization problem, this equation allows us to relate it with the level-set function. In order to achieve an iterative procedure, the value of the characteristic function is chosen to be fixed with the level-set function of the previous iteration,

$$\chi^i(\boldsymbol{X})=H\left(\omega^{i-1}\left(\boldsymbol{X}\right)\right) \tag{6.26}$$

Once the characteristic function is defined for iteration i, we are able to solve the Nonlinear Solid Mechanics problems 6.16 taking into account that the constitutive tensor is now split as a function of χ^i. Straightaway we compute the numerical approach of the topological derivative $D_T^i(\boldsymbol{X},\chi^i)$ stated at equation 6.9(without taking into account the constant K) and the signed topological derivative $\overline{D}_T^i(\boldsymbol{X},\chi^i)$ according with expression 6.19.

Expression 6.21 allows us to compute the value of the level-set function for iteration i. However, due to convergence aspects, it is needed to introduce a relaxation scheme to compute an intermediate function, $\pi^i(\boldsymbol{X},\chi^i)$ such that

$$\pi^i(\boldsymbol{X},\chi^i)=\kappa^i\frac{\boldsymbol{P}_h\left(\overline{D}_T^i(\boldsymbol{X},\chi^i)\right)}{\parallel\boldsymbol{P}_h\left(\overline{D}_T^i(\boldsymbol{X},\chi^i)\right)\parallel}+\left(1-\kappa^i\right)\frac{\boldsymbol{P}_h\left(\overline{D}_T^{i-1}(\boldsymbol{X},\chi^{i-1})\right)}{\parallel\boldsymbol{P}_h\left(\overline{D}_T^{i-1}(\boldsymbol{X},\chi^{i-1})\right)\parallel} \tag{6.27}$$

where $\boldsymbol{P}_h$ is the projection onto the finite element space and can be computed by using a lumped mass matrix approach for computational efficiency. The parameter κ^i is a relaxation parameter and it must be computed every iteration [18]. In this work, A heuristic approach which uses an oscillation indicator among iterations is considered ,

$$\xi^i(\boldsymbol{X},\chi^i)=\ \text{sign}\left(\frac{\widetilde{\pi}^i(\boldsymbol{X},\chi^i)-\pi^{i-1}(\boldsymbol{X},\chi^{i-1})}{\pi^{i-1}(\boldsymbol{X},\chi^{i-1})-\pi^{i-2}(\boldsymbol{X},\chi^{i-2})}\right) \tag{6.28}$$

where $\widetilde{\pi}^i(\boldsymbol{X},\chi^i)=\frac{\boldsymbol{P}_h\left(\overline{D}_T^i(\boldsymbol{X},\chi^i)\right)}{\|\boldsymbol{P}_h\left(\overline{D}_T^i(\boldsymbol{X},\chi^i)\right)\|}$ is the normalized value of the projection of the signed topological derivative which will allow us to predict the behaviour of the method with respect to the previous iterations.

Thus, the indicator becomes 1 when the iterative procedure behaves monotonically with the two previous iterations and it turns -1 when there exists an oscillation among previous iterations. According with [18], if there are oscillations $\left(\xi^i(\boldsymbol{X},\chi^i)=-1\right)$ then the relaxation

parameter κ^i must be decreased according with the previous ones whilst when $\left(\xi^i(\boldsymbol{X},\chi^i)=1\right)$ no oscillations are presented and the value for κ^i can be increased up to a maximum of 1. The scalar value of κ^i is then computed as:

$$\kappa^i = \min\left[\left(\frac{\int_\Omega \left(\mu^i(\boldsymbol{X},\chi^i)\right)^{c_c} d\Omega}{\int_\Omega \left(\mu^i(\boldsymbol{X},\chi^i)\right) d\Omega}\right)^{-c_c}, 1\right] \tag{6.29}$$

where $\mu^i(\boldsymbol{X},\chi^i)$ is a function which depends upon the oscillations

$$\mu^i(\boldsymbol{X},\chi^i) = \begin{cases} c_a\kappa^{i-1} & \text{if } \xi^i(\boldsymbol{X},\chi^i)=1 \\ c_b\kappa^{i-1} & \text{if } \xi^i(\boldsymbol{X},\chi^i)=-1 \end{cases} \tag{6.30}$$

where $c_a \geq 1$, $c_b \leq 1$ and $c_c \leq 1$ are algorithmic parameters which make the relaxation parameter κ^i decrease or increase up depending upon the oscillations with the previous iterations. Once κ^i is computed, the intermediate function $\pi^i(\boldsymbol{X},\chi^i)$ is easily reckoned and the level-set function for iteration i can be defined as

$$\omega^i\left(\boldsymbol{X},\chi^i\right) = \pi^i(\boldsymbol{X},\chi^i) + \alpha^i \tag{6.31}$$

where the scalar parameter α^i is computed with a secant method to fulfill the volume constraint through equation 6.22. The iterative procedure stops when after several iterations the functional to be minimized, the structural compliance defined by the external forces $W_{\boldsymbol{f}_{\text{ext}}}$, has not changed a certain percentage of its value.

To end up this section let us write down the algorithm for the Topology Optimization problem of Nonlinear Solid Mechanics:

Algorithm 2: Flowchart for Topological-Derivative based Topology Optimization of Nonlinear Structures

---

1. Set all the constant values and initial variables,
   (a) Algorithmic parameters, c_a, c_b, c_c.
   (b) Level-set function, $\omega^0 = 1$.
   (c) Relation between soft and stiff material, δ.
   (d) Desired fraction for the final volume of the structure, L.
   (e) The projection onto the finite element space $\boldsymbol{P}_h$ which in our work is computed as

a lumped mass matrix

$$\boldsymbol{P}_h \simeq \boldsymbol{M}_{\text{lumped}} = M_{ijIJ} = \delta_{ij} \int_{\Omega} \rho N_I N_I d\Omega$$

2. Here it starts the iterative procedure for the topological optimization, iteration i

   (a) Compute the characteristic function χ^i by using the Heaviside function $H(\omega)$, equation 6.23.

   $$\chi^i(\boldsymbol{X}) = H\left(\omega^{i-1}(\boldsymbol{X})\right)$$

   (b) Compute the split constitutive tensor, taking into account that the soft material behaves simulating absence of material (Equation 6.15) and the stiff material constitutive tensor comes from the Constitutive model considered, Section 3.

   $$\mathbb{C} = \chi^i \mathbb{C}^+ + (1-\chi^i)\mathbb{C}^-$$

   (c) Now it is needed to solve the Nonlinear Solid Mechanics problem. We refer to Algorithm 1 to solve it with a Newton-Raphson procedure and using the Newmark β-method as time integrator if a transient problem is considered.

   (d) It is time to reckon the signed topological derivative for the already converged structure,

   $$\overline{D_T}(\boldsymbol{X}, \chi^i) = \begin{cases} +\boldsymbol{S}^i : \boldsymbol{E}^i & \text{if } \chi^i = 1 \\ -\boldsymbol{S}^i : \boldsymbol{E}^i & \text{if } \chi^i = 0 \end{cases}$$

   (e) To figure out the level-set function, we need to split among the first two time steps and the other ones

      i. If $i < 3$ then

         A. The relaxation parameter is fixed as one, $\kappa^i = 1$, and the intermediate function is computed only as a function of the characteristic value of iteration i

         $$\pi^i(\boldsymbol{X}, \chi^i) = \kappa^i \frac{P_h\left(\overline{D}_T^i(\boldsymbol{X}, \chi^i)\right)}{\| P_h\left(\overline{D}_T^i(\boldsymbol{X}, \chi^i)\right) \|}$$

         B. Solve with the secant method, the following equation

         $$\int_{\Omega} H\left[\omega^i\left(\boldsymbol{X}, \chi^i\right)\right] d\Omega = \int_{\Omega} H\left[\pi^i(\boldsymbol{X}, \chi^i) + \alpha^i\right] d\Omega = L \mid \Omega \mid \underset{\text{secant method}}{\Longrightarrow} \alpha^i$$

C. The level-set function emerges as

$$\omega^i\left(\boldsymbol{X},\chi^i\right)=\pi^i(\boldsymbol{X},\chi^i)+\alpha^i$$

ii. If $i\geq 3$ then

A. Compute the oscillator indicator

$$\xi^i(\boldsymbol{X},\chi^i)=\ \text{sign}\ \left(\frac{\widetilde{\pi}^i(\boldsymbol{X},\chi^i)-\pi^{i-1}(\boldsymbol{X},\chi^{i-1})}{\pi^{i-1}(\boldsymbol{X},\chi^{i-1})-\pi^{i-2}(\boldsymbol{X},\chi^{i-2})}\right)$$

B. Reckon function μ^i as,

$$\mu^i(\boldsymbol{X},\chi^i)=\begin{cases}c_a\kappa^{i-1} & \text{if } \xi^i(\boldsymbol{X},\chi^i)=1\\ c_b\kappa^{i-1} & \text{if } \xi^i(\boldsymbol{X},\chi^i)=-1\end{cases}$$

C. The relaxation parameter emerges as

$$\kappa^i=\min\left[\left(\frac{\int_\Omega\left(\mu^i(\boldsymbol{X},\chi^i)\right)^{c_c}d\Omega}{\int_\Omega\left(\mu^i(\boldsymbol{X},\chi^i)\right)d\Omega}\right)^{-c_c},1\right]$$

D. And the intermediate function is now easily computed with the signed topological derivative of both this iterations and the previous one

$$\pi^i(\boldsymbol{X},\chi^i)=\kappa^i\frac{\boldsymbol{P}_h\left(\overline{D}_T^i(\boldsymbol{X},\chi^i)\right)}{\parallel\boldsymbol{P}_h\left(\overline{D}_T^i(\boldsymbol{X},\chi^i)\right)\parallel}+\left(1-\kappa^i\right)\frac{\boldsymbol{P}_h\left(\overline{D}_T^{i-1}(\boldsymbol{X},\chi^{i-1})\right)}{\parallel\boldsymbol{P}_h\left(\overline{D}_T^{i-1}(\boldsymbol{X},\chi^{i-1})\right)\parallel}$$

E. Solve with the secant method, the following equation

$$\int_\Omega H\left[\omega^i\left(\boldsymbol{X},\chi^i\right)\right]d\Omega=\int_\Omega H\left[\pi^i(\boldsymbol{X},\chi^i)+\alpha^i\right]d\Omega=L\mid\Omega\mid\underset{\text{secant method}}{\Longrightarrow}\alpha^i$$

F. The level-set function emerges as

$$\omega^i\left(\boldsymbol{X},\chi^i\right)=\pi^i(\boldsymbol{X},\chi^i)+\alpha^i$$

(f) Check convergence criterion. In our case, we compute the structural compliance and compare it with the previous one. If this value is not close enough (with regards to a tolerance value), then we start another Topology Optimization iteration by repeating the procedure from step 2.

Chapter 7

Numerical Examples

7.1 Validation

In order to check the correctness of our implementation to see wether our method is capable of reproducing correct results, it is wanted to perform some numerical examples found in the literature to obtain similar results. Let us show two benchmark examples in the Topology Optimization field.

7.1.1 Clamped Clamped Beam

In this example a Clamped Clamped Beam under plane stress state is considered. The initial beam considered (Reference Domain) is defined by the rectangular domain shown in Figure 7.1 where $L = 20$ mm. A punctual force $F = 30$ N is applied in the middle of the lower bound.

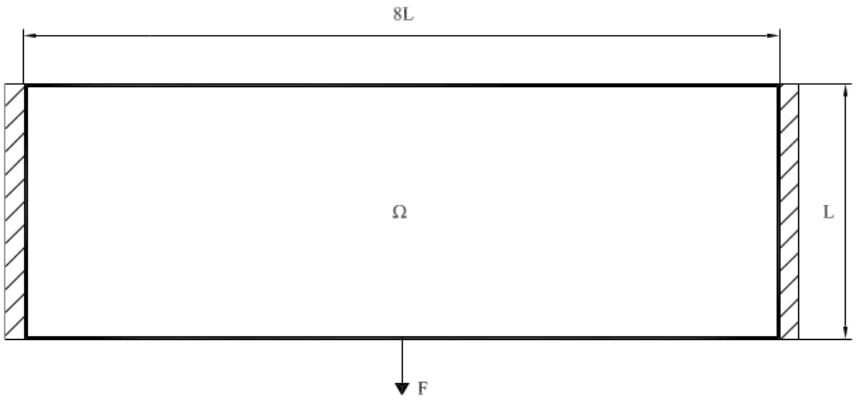

Figure 7.1: Clamped Clamped Beam Initial Domain. From [7]

As a Constitutive Model, the Saint Venant-Kirchhoff Material is considered. Thus, material properties are properly defined with a Young Modulus $E = 30\frac{\text{N}}{\text{mm}^2}$ and a Poisson's coeffi-

cient $\nu = \frac{1}{3}$. The same example is performed in [2, 7, 16]. A mesh of 29.392 linear elements is built to perform the analysis. As a final volume (area in this case) a 0.2 of the initial volume is imposed.

Let us show the evolution of the optimal structure for this load case,

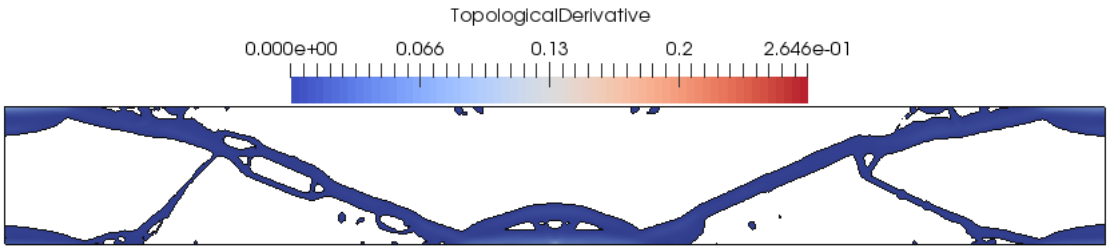

(a) Iteration 1

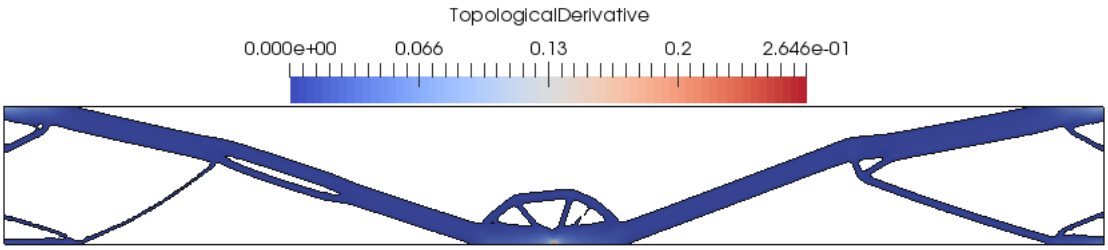

(b) Iteration 2

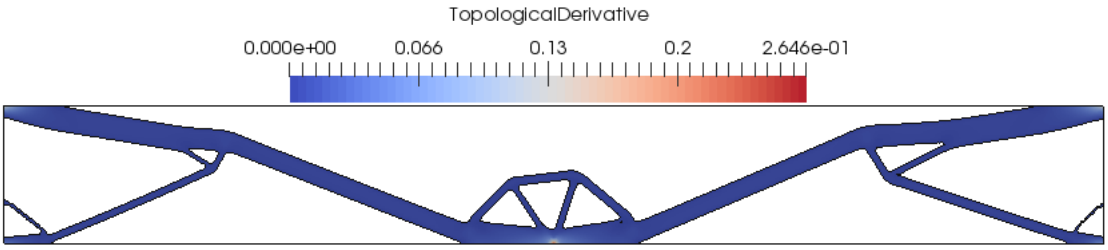

(c) Iteration 10

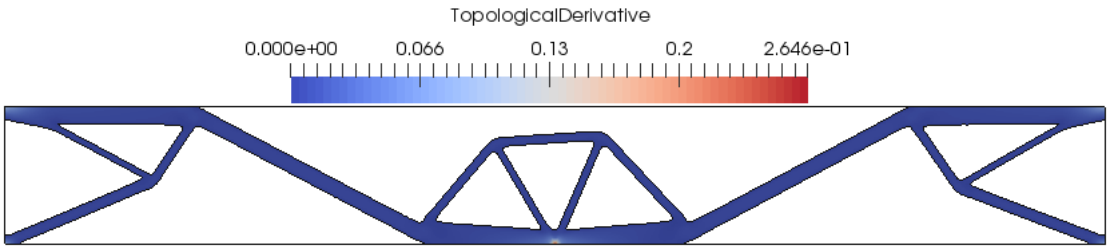

(d) Iteration 30

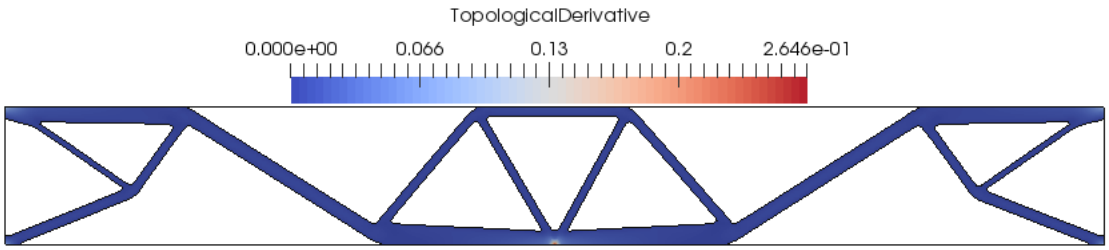

(e) Iteration 55

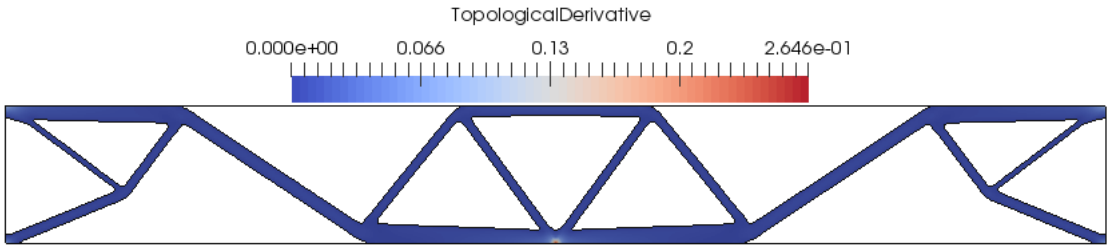

(f) Iteration 100

Figure 7.2: Evolution of the Optimal Clamped Clamped Beam with the iterative Topology Optimization algorithm

Figure 7.2 displays the evolution of the optimal structure. As expected the maximum values of the topological derivatives appear in the loading point and the areas where the structure is clamped. The problem is left to be running up to iteration 100 to show that the structure has achieved a stable solution which satisfies the volume constraint and the topology remains almost constant from iteration 55.

As commented previously, this example was also run by [2, 7, 16] obtaining the following final topology:

Figure 7.3: Final Optimal Structure for the Clamped Clamped Beam found by [7, 16]. From [7]

Both solutions are practically identical, so we can validate our code. Regarding to the difference among our algorithm and the iterative procedure proposed by [2, 7, 16], they remove a percentage of the volume at each iteration and do not allow an element to change between stiff material or soft material once the element has been removed. In our case, we impose the

volume constraint at each iteration by adding a scalar in the level set function and the method allows elements to freely change its properties untill convergence is achieved.

To end up this example, let us show the displacement field for the final structure,

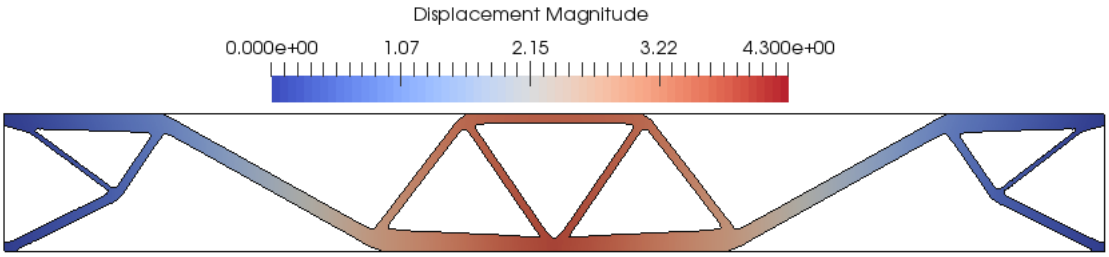

Figure 7.4: Displacement Field for the Final Structure

In figure 7.4 it can be seen the displacement magnitude for the final structure. As expected, maximum values appear where the force is applied. The areas which are in contact with the lateral boundaries present null displacement due to the clamped boundary condition. To end up, let us remark that the displacements represent more or less 20% of the minor length, which ensures us that the large displacements region has been surpassed.

7.1.2 Cantilever Beam

In this example, the aim is to obtain the optimal structure of a Cantilever Beam with a force $F = 7500$ N applied on the free end large enough to cause large rotations on the structure. As an initial Reference Domain it is taken also a rectangular domain . The upper and lower part of the left boundary are considered clamped while the rest is free. The rest of the boundaries remains also without restrictions. Figure (7.5) shows the initial configuration of the problem. $L = 50$ mm and $a = 5$ mm.

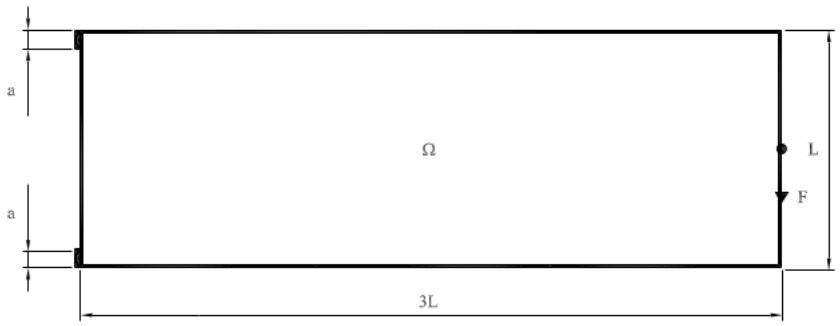

Figure 7.5: Cantilever Beam Initial Domain. From [7]

As a Constitutive Model, it is also considered the Saint Venant-Kirchhoff Material. Thus, material properties are properly defined with a Young Modulus $E = 210 \cdot 10^3 \frac{\text{N}}{\text{mm}^2}$ and a Poisson's coefficient $\nu = 0.25$. The same example is performed in [2, 7, 16]. A mesh of 17182 linear elements is built to perform the analysis. As a final volume (area in this case) a 0.32 of the initial volume is imposed.

Let us show the evolution of the optimal structure for this load case,

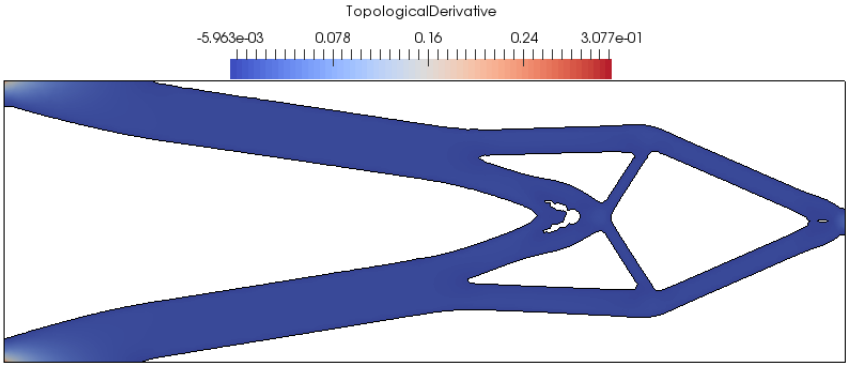

(a) Iteration 1

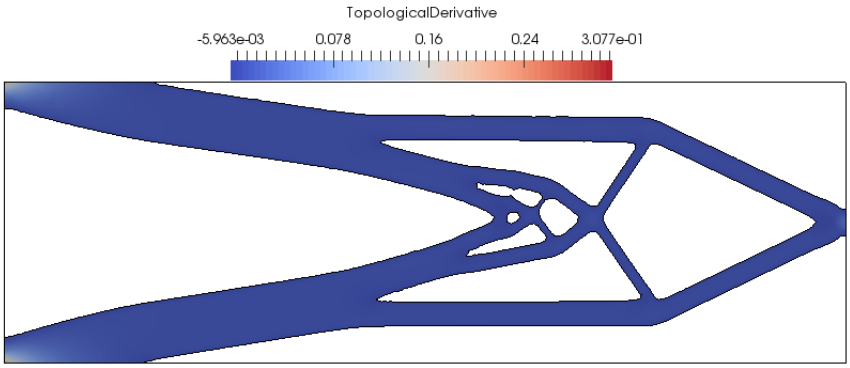

(b) Iteration 2

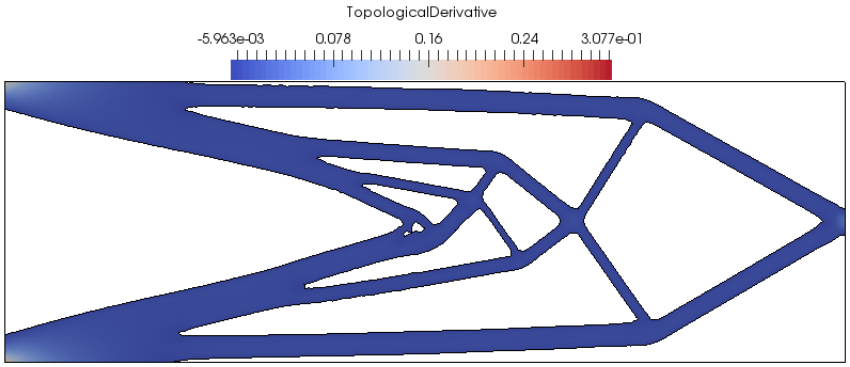

(c) Iteration 10

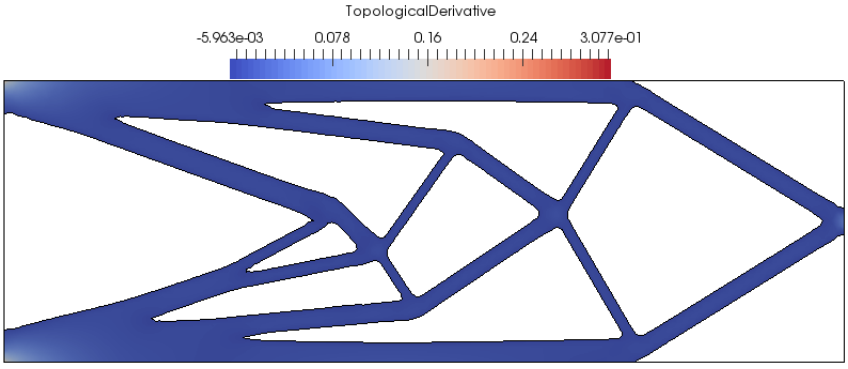

(d) Iteration 20

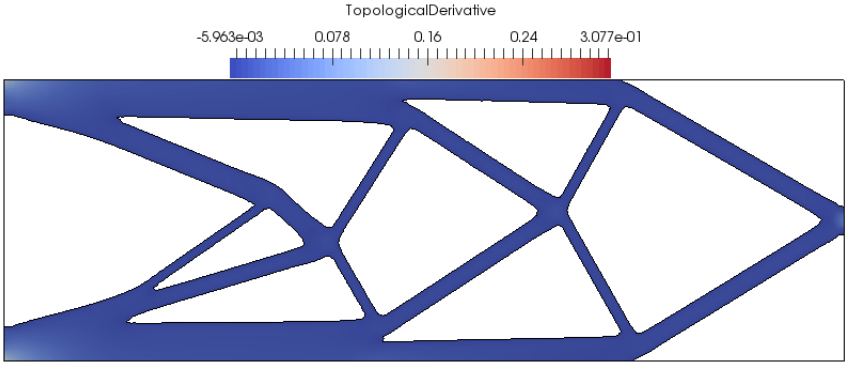

(e) Iteration 40

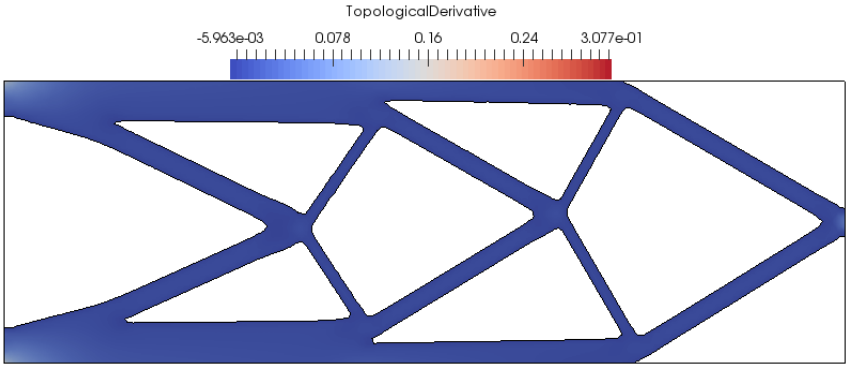

(f) Iteration 60

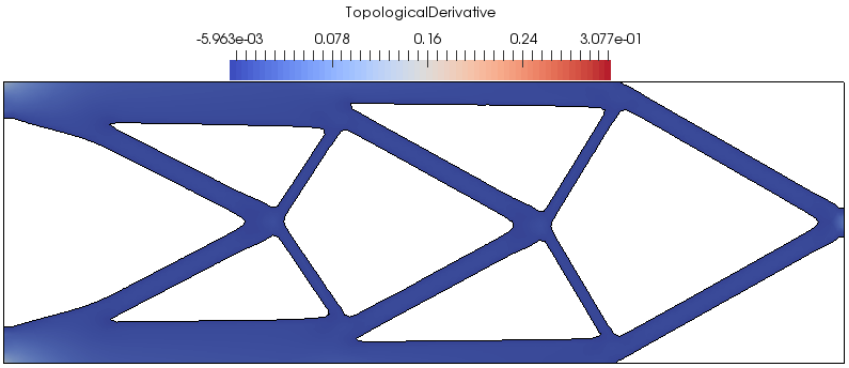

(g) Iteration 100

Figure 7.6: Evolution of the Optimal Cantilever Beam with the iterative Topology Optimization algorithm

Figure 7.6 shows evolution of the cantilever beam to the optimal structure according with our iterative algorithm. As expected the maximum values of the topological derivatives appear in the loading point and the areas where the structure is clamped. The problem is left to be running up to iteration 100 to show that the structure has achieved a stable solution which satisfies the volume constraint and the topology remains almost constant from iteration 60.

This problem was also solved by [7] obtaining the following final structure:

Figure 7.7: Final Optimal Structure for the Cantilever Beam found by [7]. From [7]

Comparing both solutions we can conclude that very similar results have been obtained. Finally, to end up this section, let us show the final displacement field,

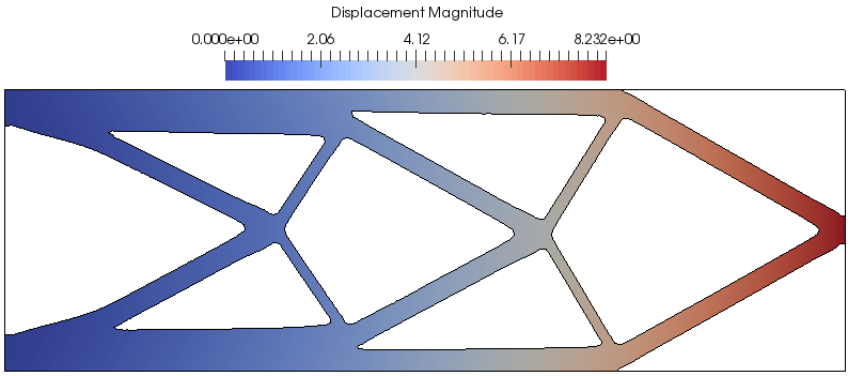

Figure 7.8: Displacement Field for the Final Cantilever Beam

In figure 7.8 it can be observed the final displacement field for the proposed Cantilever Beam. As it was expected, maximum displacements appear where the external force is applied. It can also be seen that the clamped boundary remains with null displacement. To end up, let us remark that the maximum displacement corresponds approximately to 20% of the domain height.

7.2 Engineering Cases

Once our code has been validated, it is time to apply it to some interesting engineering cases to develop the optimal structure for a given set of external conditions.

7.2.1 Bridge Design

Let us consider now a bridge design. The reference domain $\widetilde{D}$ is given by a rectangle of size 180 m times 60 m supported on the two opposites bottom corners of equal length $a = 9$ m. To simulate the traffic loading over the bridge deck it is considered a distributed loading $\boldsymbol{g} = (0.0, -4)\ \frac{\text{KN}}{\text{m}}$ applied on the horizontal line in the middle of the reference domain. In addition it is imposed that the bridge deck is only allowed to move horizontally. See the sketch in Figure 7.9 .The material properties for a Saint Venant-Kirchhoff Material model are $E = 240$ MPa and $\nu = 0.2$.

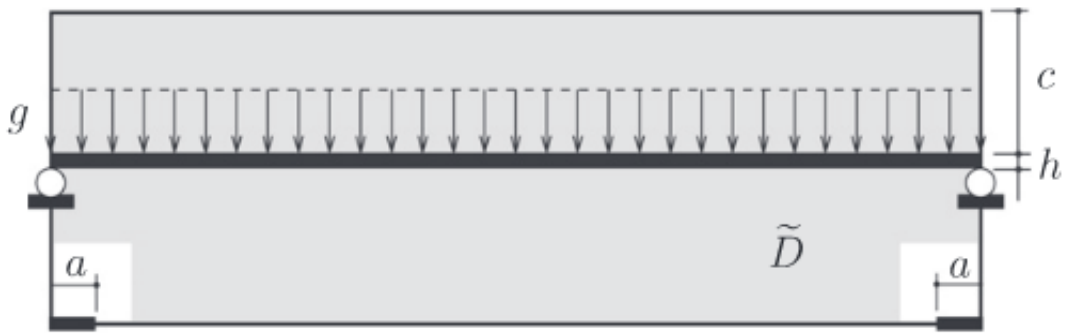

Figure 7.9: Bridge Design. Initial Domain and boundary conditions.

The final optimal bridge design taking into account a final volume fraction of 40% emerges as,

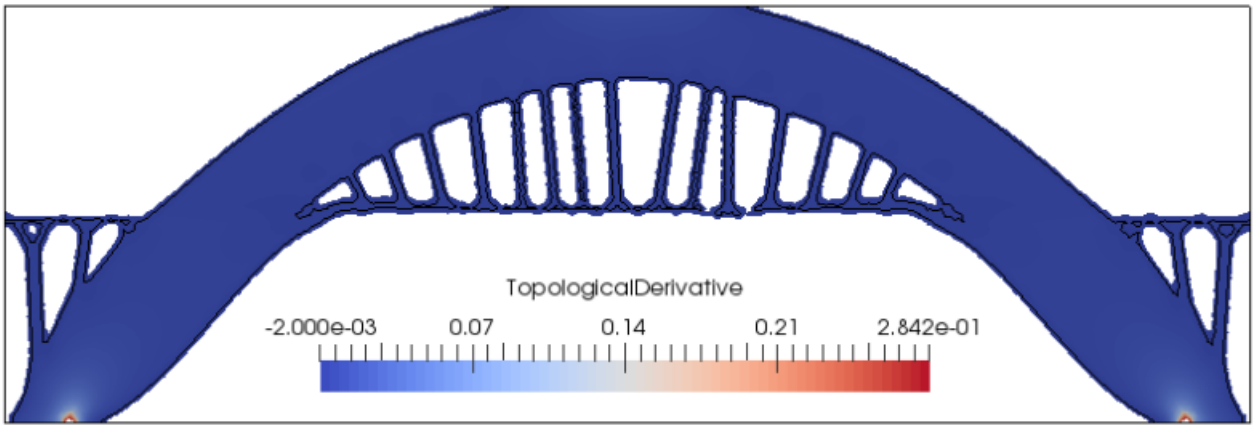

Figure 7.10: Bridge Design.Optimal Design.

7.2.2 L-Bracket Design

Let us now move to a classical structural optimization problem, the L-bracket problem. The problem consists in considering as a reference domain $\widetilde{D}$ as the one shown in figure 7.9. The lengths of the horizontal and vertical branches are respectively 2 m and 2.5 m. The structure is clamped at the top edge and a point load $g = 40$ KN is applied to the above corner of the right boundary. It is considered $E = 12.5$ MPa and $\nu = 0.2$ as a material properties of the Saint Venant-Kirchhoff material model.

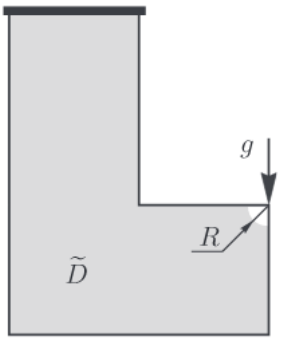

Figure 7.11: L-Bracket Design. Initial Domain and boundary conditions.

Considering as a final volume a fraction of 40% of the initial reference domain it is obtained as a final structure,

(a) Linear Case (b) NonLinear Case

Figure 7.12: L-Bracket Design.Optimal Design.

Figure 7.11 displays the optimal solution for both linear and nonlinear cases. As expected linear case matches with the ones stated in the literature. Regarding to the Nonlinear case, it can be seen that a more complex structure than the one obtained for linear elasticity is achieved due to the extreme nonlinearity of the problem.

Chapter 8

Conclusions

8.1 Final Remarks

In this thesis a new method to perform Topology Optimization of Nonlinear Structures by means of the Topological Derivative concept has been presented. The application consists in using the Topological Sensitivity Analysis with the expression for the Topological Derivative in nonlinear scenarios. Although the analytical expression can not be calculated, a numerical expression coming from the literature has been applied giving validated results.

With regards to the Topology Optimization process, an iterative computation coupled with a level set strategy to impose the volume constraint has been explained. The level-set allows us to keep a sharp tracking of the interface between the stiff and soft material, which in our case represent those areas with material and those which will be considered void.

As a main differences between this iterative procedure to find the optimal structure and the ones already performed in the literature, we can highlight :

- Whereas the majority of the iterative procedures apply the volume constraint in a decreasing way, **our iterative procedure satisfies each iteration the volume constraint** by adding a scalar to the level set method. This scalar will be in charge of ensuring this condition and must be recomputed each iteration.

- In the iterative Topology Optimization Algorithm presented in this thesis, **elements are allowed to change their material properties**, so that they can belong to the stiff material and change to soft material in the following iterations and vice versa. Most of the methods in the literature do not allow this change, so that those elements which become soft material, will remain soft material for the rest of the procedure.

- It is easy to see that **our iterative procedure will need more iterations to converge**.

However, our procedure is always imposing the same volume constraint, which will lead us to the real solution of the Topological Optimization Problem(6.17).

- **To ensure that the code will not become unstable** a relaxation scheme must be applied and the relaxation parameter must be recomputed each iteration according to some algorithmic parameters in order to control how the elements are allowed to change their material properties. This scheme allows us to see the evolution of the iterations to identify the presence of oscillations. **Depending upon the oscillations, the scheme is allowed to go faster or slower**.

Regarding to the resulting matrix of our iterative procedure, the fact of using a soft constitutive tensor very small compared with the stiff one **makes our matrix to be ill-conditioned**. Thus, it will be necessary to use some kind of preconditioner if it is wanted to use an iterative solver to solve the algebraic system of equations given by Newton's method in the Nonlinear problem.

Several benchmarks have been performed to validate our Topology Optimization algorithm for Nonlinear Structures obtaining very similar results to the ones given by the literature . To end up, two engineering cases, have been proposed to see the proper performance of the code and how powerful and helpful it could be to solve engineering problems.

8.2 Future Work

To end up this section, it is important to show different new research directions which are set through this work.

- The code is developed for both 2 and 3 dimensions. Thus, it is important to **validate the code also for 3 dimensions.**

- Currently, the code only works with Saint Venant-Kirchhoff material model. It would be important to **re-code the procedure to allow the application of other types of nonlinear elastic models.**

- Topology Optimization problem of Nonlinear Structures requires to solve one Nonlinear problem (which has to be done iteratively and applying external loads slowly) per each Topology Optimization iteration. Therefore, the problem can become huge very fast when increasing the number of unknowns. **Parallelization of the code seems to be essential to deal with this problem in mid-large scale applications.** Fortunately, `FEMUSS` runs also in parallel and the iterative procedure shown here can be parallelized.

Thus, strong and weak scalability tests should be performed to show the behavior of this algorithm in parallel.

- When the material becomes **nearly incompressible**, the displacement-based Finite Element Method ends up giving wrong approximations. To deal with this problem, **a mixed formulation must be implemented** in which a pressure-like variable is added to the problem to enforce the incompressible condition. Several mixed formulations are already stated for nonlinear cases [8, 9] using strains or stresses as unknowns. The displacement-pressure mixed formulation has been already stated for linear elasticity [4, 11] whereas it has to be studied for Total Lagrangian Formulation in Nonlinear scenarios.

- Once these tasks have been performed, it will be time to expand the Topology Optimization a little further, **Fluid-Structure Interaction**. Be able to find the optimal structure by means of the Topology Optimization when our structure (which can be considered either linear or nonlinear) is in interaction with an internal or surrounding fluid flow. The main objective will be to find the optimal structure which minimizes the work done by the tractions given by the fluid.

References

[1] A.A.Novotny, R.A.Feijóo, E.Taroco, and C.Padra. Topological sensitivity analysis. *Computer Methods in Applied Mechanics and Engineering*, 192(7):803 – 829, 2003.

[2] Francesc A.M.Gomes and Thadeu A. Senne. An algorithm for the topology optimization of geometrically nonlinear structures. *International Journal for numerical methods in engineering*, 99:391–409, 2014.

[3] Samuel Amstutz and Heiko Andru. A new algorithm for topology optimization using a level-set method. *Journal of Computational Physics*, 216:573–588, 2006.

[4] Joan Baiges and Ramon Codina. Variational multiscale error estimators for solid mechanics adaptive simulations: an orthogonal subgrid scale approach. *Computer Methods in Applied Mechanics in Engineering*, 325:37–55, 2017.

[5] Ted Belytschko, Wing Kam Liu, and Brian Moran. *Nonlinear Finite Elements for Continua and Structures*. Wiley, 2000.

[6] Javier Bonet and Richard D.Wood. *Nonlinear Continuum Mechanics for Finite Element Analysis*. Cambridge University Press, 1997.

[7] C.E.L.Pereira and M.L.Bittencourt. Topological sensitivity analysis in large deformation problems. *Structural and Multidisciplinary Optimization*, 37:149–163, 2008.

[8] M. Cervera, M.Chiumenti, and R. Codina. Mixed stabilized finite element methods in nonlinear solid mechanics. part i: Formulation. *Computer Methods in Applied Mechanics in Engineering*, 199:2559–2570, 2010.

[9] M. Cervera, M.Chiumenti, and R. Codina. Mixed stabilized finite element methods in nonlinear solid mechanics. part ii: Strain localization. *Computer Methods in Applied Mechanics in Engineering*, 199:2571–2589, 2010.

[10] Feifei Chen, Yiqiang Wang, Michael Yu Wang, and Y.F.Zhang. Topology optimization of hyperelastic structures using a level set method. *Journal of Computational Physics*, 351:437–454, 2017.

[11] M. Chiumenti, Q.Valverde, C.Agelet de Saracibar, and M.Cervera. A stabilized formulation for incompressible elasticity using linear displacement and pressure interpolations. *Computer Methods in Applied Mechanics in Engineering*, 191:5253–5264, 2002.

[12] Anders Clausen, Niels Aage, and Ole Sigmund. Topology optimization of coated structures and material interface problems. *Computer Methods in Applied Mechanics and Engineering*, 290:524 – 541, 2015.

[13] Robert C.Martin. *Clean Code: A handbook of Agile Software Craftsmanship*. Prentice Hall, 2008.

[14] Cinthia G.Lopes, Renatha B. dos Santos, and Antonio A.Novotny. Topological derivative-based topology optimization of structures subject to multiple load-cases. *Latin American Journal of Solids and Structures*, 12(5):834–860, 2015.

[15] Seung-Hyun Ha and Seonho Cho. Level set based topological shape optimization of geometrically nonlinear structures using unstructured mesh. *Computers and Structures*, 86:1447–1455, 2008.

[16] Daeyoon Jung and Hae Chang Gea. Topology optimization of nonlinear structures. *Finite Elements in Analysis and Design*, 40(11):1417 – 1427, 2004.

[17] A. Klarbring and N. StrÃ¶mberg. Topology optimization of hyperelastic bodies including non-zero prescribed displacements. *Structural and Multidisciplinary Optimization*, 41(1):37–48, 2013.

[18] A. Lambde and A.Czekanski. Topology optimization using a continuous density field and adaptive mesh refinement. *International Journal for Numerical Methods in Engineering*, 113:357–373, 2018.

[19] Yangjun Luo, Ming Li, and Zhan Kang. Topology optimization of hyperelastic structures with frictionless contact supports. *International Journal of Solids and Structures*, 81:373 – 382, 2016.

[20] J.A. Norato, M.P. Bendsøe, and R.B. et al. Haber. A topological derivative method for topology optimization. *Structural and Multidisciplinary Optimization*, 33:375–386, 2007.

[21] Xavier O. Olivella and Carlos A. de Saracibar Bosch. *Continuum Mechanics for Engineers. Theory and Problems*. CC-BY-NC-ND, 2017.

[22] Sergio Oller. *Nonlinear Dynamics of Structures*. Springer, 2014.

[23] Jaejong Park and Alok Sutradhar. A multi-resolution method for 3d multi-material topology optimization. *Computer Methods in Applied Mechanics and Engineering*, 285:571 – 586, 2015.

[24] Martin P.Bendsøe and Ole Sigmund. *Topology Optimization. Theory, Methods and Applications*. Springer, 2002.

[25] James W.Newkirk Robert C.Martin and Robert S.Koss. *Agile Software Development: Principles, Patterns and Practices*. Prentice Hall, 2002.

[26] Ole Sigmund and Kurt Maute. Topology optimization approaches: A comparative review. *Structural and Multidisciplinary Optimization*, 48:1031–1055, 2013.

[27] Michael Yu Wang, Xiaoming Wang, and Dongming Guo. A level set method for structural topology optimization. *Computer Methods in Applied Mechanics and Engineering*, 192(1):227 – 246, 2003.

Appendix A

Mathematical Theorems

A.1 Gauss's theorem

This theorem relates integrals over a domain to an integral over the boundary of this domain. The one-dimensional form of Gauss's theorem is the so-called fundamental theorem of calculus.

Consider a function $f(\boldsymbol{x})$ piecewise continuously differentiable. That is equivalent to say $f(\boldsymbol{x}) \in C^0(\boldsymbol{x})$, then

$$\int_{\Omega} \frac{\partial f(\boldsymbol{x})}{\partial x_i} d\Omega = \int_{\Gamma} n_i f(\boldsymbol{x}) d\Gamma \qquad \text{or} \qquad \int_{\Omega} \nabla f(\boldsymbol{x}) d\Omega = \int_{\Gamma} \boldsymbol{n} f(\boldsymbol{x}) d\Gamma \tag{A.1}$$

where Ω is the integration domain, Γ is the boundary of this domain and $\boldsymbol{n}$ is the outward normal vector. This theorem holds for any domain, including the reference domain Ω_0. The above theorem also holds for a tensor of any order; for example if we replace the scalar function $f(\boldsymbol{x})$ by a tensor of first order $\boldsymbol{g}(\boldsymbol{x})$, then

$$\int_{\Omega} \frac{\partial g_i(\boldsymbol{x})}{\partial x_i} d\Omega = \int_{\Gamma} n_i g_i(\boldsymbol{x}) d\Gamma \qquad \text{or} \qquad \int_{\Omega} \nabla \cdot \boldsymbol{g}(\boldsymbol{x}) d\Omega = \int_{\Gamma} \boldsymbol{n} \cdot \boldsymbol{g}(\boldsymbol{x}) d\Gamma \tag{A.2}$$

which is often known as the divergence theorem. The theorem can be also applied to gradients of the vector field,

$$\int_{\Omega} \frac{\partial g_i(\boldsymbol{x})}{\partial x_j} d\Omega = \int_{\Gamma} n_j g_i(\boldsymbol{x}) d\Gamma \qquad \text{or} \qquad \int_{\Omega} \nabla \boldsymbol{g}(\boldsymbol{x}) d\Omega = \int_{\Gamma} \boldsymbol{n} \otimes \boldsymbol{g}(\boldsymbol{x}) d\Gamma \tag{A.3}$$

A.2 Material time derivative of an integral and Reynold's transport theorem

The rate of change of an integral on a material domain is the material time derivative of an integral. No mass flux occurs across the boundaries due to the fact that the material domain moves with the material. The material time derivative of an integral is defined by

$$\frac{D}{Dt}\int_{\Omega} f(\boldsymbol{x},t)\,d\Omega = \lim_{\triangle t\to 0}\frac{1}{\triangle t}\left(\int_{\Omega_{\tau+\triangle t}} f(\boldsymbol{x},\tau+\triangle t)\,d\Omega - \int_{\Omega_{\tau}} f(\boldsymbol{x},\tau)\,d\Omega\right) \tag{A.4}$$

Reynold's transport theorem states that

$$\frac{D}{Dt}\int_{\Omega} f(\boldsymbol{x},t)\,d\Omega = \int_{\Omega}\left(\frac{Df(\boldsymbol{x},t)}{Dt} + f(\boldsymbol{x},t)\,\frac{\partial v_i}{\partial x_i}\right)d\Omega \tag{A.5}$$

An alternative form of Reynold's transport theorem gives

$$\frac{D}{Dt}\int_{\Omega} f(\boldsymbol{x},t)\,d\Omega = \int_{\Omega}\left(\frac{\partial f(\boldsymbol{x},t)}{\partial t} + \text{ div }(\boldsymbol{v}f)\right)d\Omega \tag{A.6}$$

Let us recall that Reynold's transport theorem can be applied to any tensor order by replacing the scalar function $f(\boldsymbol{x})$ by the tensor itself.

Appendix B

Voigt Notation

B.1 Voigt rule applied to second-order tensors

In finite element methods, symmetric second-order tensors are often written as column matrices. The Voigt rule depends on whether a tensor is a kinetic quantity, such as a stress, or a kinematic quantity, such as a strain.

B.1.1 Kinetic Voigt rule

Let us consider a symmetric second order tensor $\boldsymbol{\sigma}$, the Voigt rule for this kinetic tensor is

$$\boldsymbol{\sigma} \equiv \begin{bmatrix} \sigma_{11} & \sigma_{12} \\ \text{sym} & \sigma_{22} \end{bmatrix} \longrightarrow \begin{Bmatrix} \sigma_{11} \\ \sigma_{22} \\ \sigma_{12} \end{Bmatrix} = \begin{Bmatrix} \sigma_1 \\ \sigma_2 \\ \sigma_3 \end{Bmatrix} \equiv \{\boldsymbol{\sigma}\} \quad \text{in 2D} \tag{B.1}$$

and

$$\boldsymbol{\sigma} \equiv \begin{bmatrix} \sigma_{11} & \sigma_{12} & \sigma_{13} \\ & \sigma_{22} & \sigma_{23} \\ \text{sym} & & \sigma_{33} \end{bmatrix} \longrightarrow \begin{Bmatrix} \sigma_{11} \\ \sigma_{22} \\ \sigma_{33} \\ \sigma_{12} \\ \sigma_{13} \\ \sigma_{23} \end{Bmatrix} = \begin{Bmatrix} \sigma_1 \\ \sigma_2 \\ \sigma_3 \\ \sigma_4 \\ \sigma_5 \\ \sigma_6 \end{Bmatrix} \equiv \{\boldsymbol{\sigma}\} \quad \text{in 3D} \tag{B.2}$$

Any tensor or matrix converted by the Voigt rule is said to be in Voigt form, and is enclosed by brackets as shown above.

B.1.2 Kinematic Voigt rule

Let us consider a symmetric second order tensor $\boldsymbol{\varepsilon}$, the Voigt rule for this kinematic tensor is

$$\boldsymbol{\varepsilon} \equiv \begin{bmatrix} \varepsilon_{11} & \varepsilon_{12} \\ \text{sym} & \varepsilon_{22} \end{bmatrix} \longrightarrow \begin{Bmatrix} \varepsilon_{11} \\ \varepsilon_{22} \\ 2\varepsilon_{12} \end{Bmatrix} = \begin{Bmatrix} \varepsilon_1 \\ \varepsilon_2 \\ \varepsilon_3 \end{Bmatrix} \equiv \{\boldsymbol{\varepsilon}\} \quad \text{in 2D} \tag{B.3}$$

and

$$\boldsymbol{\varepsilon} \equiv \begin{bmatrix} \varepsilon_{11} & \varepsilon_{12} & \varepsilon_{13} \\ & \varepsilon_{22} & \varepsilon_{23} \\ \text{sym} & & \varepsilon_{33} \end{bmatrix} \longrightarrow \begin{Bmatrix} \varepsilon_{11} \\ \varepsilon_{22} \\ \varepsilon_{33} \\ 2\varepsilon_{12} \\ 2\varepsilon_{13} \\ 2\varepsilon_{23} \end{Bmatrix} = \begin{Bmatrix} \varepsilon_1 \\ \varepsilon_2 \\ \varepsilon_3 \\ \varepsilon_4 \\ \varepsilon_5 \\ \varepsilon_6 \end{Bmatrix} \equiv \{\boldsymbol{\varepsilon}\} \quad \text{in 3D} \tag{B.4}$$

The factor of 2 on the shear strains results from the requirement that the expressions for the energy be equivalent in Voigt notation and inditial notation. It is easy to verify that the following expressions are equal:

$$\boldsymbol{\varepsilon} : \boldsymbol{\sigma} = \{\boldsymbol{\varepsilon}\}^T \cdot \{\boldsymbol{\sigma}\} \tag{B.5}$$

where $\boldsymbol{A} : \boldsymbol{B}$ is the double contraction of two matrices, $\boldsymbol{A} : \boldsymbol{B} = A_{ij}B_{ij}$.

B.2 Voigt Rule applied to high-order tensors

The Voigt rule is particularly useful for converting fourth-order tensors, which are awkward to implement in programming, to second-order tensors. For example the hyperelastic law in inditial notation which relates stresses to strains involves the fourth-order tensor $\mathbb{C}_{ijkl}$:

$$S_{ij} = \mathbb{C}_{ijkl}E_{kl} \qquad \text{or} \qquad \boldsymbol{S} = \mathbb{C} : \boldsymbol{E}$$

This operation reduces to a matrix-vector product in Voigt form as

$$\boldsymbol{S} = \mathbb{C} : \boldsymbol{E} \longrightarrow \{\boldsymbol{S}\} = \{\mathbb{C}\} \cdot \{\boldsymbol{E}\}$$

The transformation is made by considering $\{\mathbb{C}\}_{ab} \longrightarrow \mathbb{C}_{ijkl}$ where $ij \rightarrow a$ and $kl \rightarrow b$ following the next table.

$\{\mathbb{C}\}_{ab} \longrightarrow \mathbb{C}_{ijkl}$					
i	j → a		k	l → b	
1	1	1	1	1	1
2	2	2	2	2	2
1	2	3	1	2	3

$\{\mathbb{C}\}_{ab} \longrightarrow \mathbb{C}_{ijkl}$					
i	j → a		k	l → b	
1	1	1	1	1	1
2	2	2	2	2	2
3	3	3	3	3	3
1	2	4	1	2	4
1	3	5	1	3	5
2	3	6	2	3	6

Table B.1: Voigt rule 2D (left) and 3D (right)